Therapeutic strategies to restore intratumoral immune activity in human cancer

Kaptein, P.

Chapter 5

CD8-targeted IL2 unleashes tumor-specific immunity in human cancer tissue by reviving the dysfunctional T cell pool

Paulien Kaptein[1], Nadine Slingerland[1*], Christina Metoikidou[1*], Felix Prinz[1,2], Simone Brokamp[1], Mercedes Machuca-Ostos[1,3], Guido de Roo[4], Ton N. M. Schumacher[5,6], Yik A. Yeung[7], Kelly D. Moynihan[7], Ivana M. Djuretic[7], Daniela S. Thommen[1**]

[1] Division of Molecular Oncology and Immunology, The Netherlands Cancer Institute, Amsterdam, The Netherlands

[2] Division of Oncology, Department of Internal Medicine, Medical University of Graz, Graz, Austria

[3] Division of Tumor Biology and Immunology, The Netherlands Cancer Institute, Amsterdam, The Netherlands

[4] Flow Cytometry Facility, The Netherlands Cancer Institute, Amsterdam, The Netherlands

[5] Division of Molecular Oncology and Immunology, Oncode Institute, The Netherlands Cancer Institute, Amsterdam, The Netherlands

[6] Department of Hematology, Leiden University Medical Center, Leiden, The Netherlands

[7] Asher Biotherapeutics, Inc., South San Francisco, California

* These authors contributed equally

**Corresponding author

Published in Cancer Discovery, July 01 2024, 14(7): 1226-1251

Abstract

Tumor-specific CD8$^+$ T cells are key effectors of antitumor immunity but are often rendered dysfunctional in the tumor microenvironment. Immune checkpoint blockade can restore antitumor T cell function in some patients, however most do not respond to this therapy, often despite T cell infiltration in their tumors. We here explored a CD8-targeted IL2 fusion molecule (CD8-IL2) to selectively reactivate intratumoral CD8$^+$ T cells in patient-derived tumor fragments. Treatment with CD8-IL2 broadly armed intratumoral CD8$^+$ T cells with enhanced effector capacity, thereby specifically enabling reinvigoration of the dysfunctional T cell pool to elicit potent immune activity. Notably, the revival of dysfunctional T cells to mediate effector activity by CD8-IL2 depended on simultaneous antigen recognition and was quantitatively and qualitatively superior to that achieved by PD-1 blockade. Finally, CD8-IL2 was able to functionally reinvigorate T cells in tumors resistant to anti-PD-1, underscoring its potential as a novel treatment strategy for cancer patients.

Statement of Significance

Reinvigorating T cells is crucial for response to checkpoint blockade therapy. However, emerging evidence suggests that the PD-1/PD-L1 axis is not the sole impediment for activating T cells within tumors. Selectively targeting cytokines toward specific T cells subsets might overcome these barriers and stimulate T cells within resistant tumors.

Introduction

Over the past decade, T cell-based immunotherapies have emerged as a groundbreaking approach leveraging the potential of tumor-specific T cells to recognize and kill malignant cells[1-5]. In particular, the PD-1/PD-L1 axis has been identified as a major pathway limiting effective antitumor T cell immunity, and immune checkpoint blockade (ICB) therapies targeting this pathway have demonstrated remarkable success in reactivating tumor-specific T cells to unleash their antitumor potential[6-9]. Nevertheless, durable benefit from this treatment is currently limited to a small fraction of patients. Interestingly, T cell presence in the tumor only provides limited predictive value for response to PD-1 blockade[10-11]. This observation suggests that a considerable portion of tumors characterized by T cell infiltration remains unresponsive to ICB, and that barriers other than PD-1 signaling preventing T cell activation may exist. Hence, novel strategies are required to restore effector activity in tumor-specific T cells that are not susceptible to current ICB.

Interleukin-2 (IL2) is a powerful cytokine inducing the activation, differentiation, and proliferation of lymphocytes[12]. Notably, IL2 appears critical for the effects of PD-1 blockade, as inhibition of IL2 signaling impeded T cell activation and tumor control following PD-1 blockade in vitro and in vivo[13,14]. Furthermore, we and others previously demonstrated that addition of IL2 can overcome ICB resistance both ex vivo in human tumors and in murine tumor models[15-17] indicating its potential to improve immunotherapeutic outcomes. Systemic administration of IL2 was the first immunotherapy to be approved for the treatment of metastatic melanoma and renal cell carcinoma[18], however its clinical utilization has been challenging because of IL2's pleiotropic functions. The IL2 receptor (IL2R) consists of three receptor subunits –IL2Rα, IL2Rβ, and IL2Rγ– that together form either the intermediate-affinity dimeric IL2Rβγ present on naïve and memory T cells, and NK cells, or the high-affinity trimeric IL2Rαβγ which is strongly expressed on regulatory T (T_{reg}) cells and transiently on activated T cells[19,20]. When given at low doses, IL2 thus preferentially induces T_{reg} activation which counteracts effector T cell activity[21,22]. At higher doses IL2 can elicit immune activation and tumor control[23], but also lead to severe systemic toxicities such as inflammation and vascular leak syndrome[24,25]. While the engineering of IL2 variants (IL2v) with reduced or abolished IL2Ra binding with the goal to favor T_{eff} over T_{reg} activation[26-30] has improved toxicity issues, these molecules did not show meaningful clinical efficacy[31]. These observations suggest that non-specific targeting of all IL2Rbg-expressing cells does not provide the necessary therapeutic window to successfully exploit the clinical potential of IL2. To overcome these problems, cis-targeting of IL2 variants to T cell surface receptors has emerged as a powerful new strategy, making it possible to deliver the IL2 signal specifically to the T cell subset of interest.

We here explored a novel IL2 molecule targeted to CD8β (CD8-IL2) that allows the selective stimulation of the $CD8^+$ T cells critical for tumor control, while minimizing the activation and amplification of immunosuppressive T_{regs} and of other cell types such as NK cells that

may contribute to systemic toxicity[32]. Utilizing the patient-derived tumor fragment (PDTF) platform[10,33] that provides a tumor microenvironment (TME) context that closely resembles the one present in cancer patients, we assessed (1) whether CD8-IL2 can induce T cell activation in human tumors and which specific cell types and cell states are responsive to this treatment, (2) how CD8-IL2 reinvigorates antitumor T cell immunity, and (3) how T cell reactivation upon CD8-IL2 differs from that achieved upon PD-1 blockade. Our data demonstrate that CD8-IL2 broadly arms tumor-infiltrating $CD8^+$ T cells with effector capacity. Restoration of effector function, leading to potent immune reactivation, was most profound for the tumor-reactive dysfunctional T cell pool and required simultaneous T cell receptor (TCR) signaling. Furthermore, reinvigoration of dysfunctional T cells by CD8-IL2 was broader and qualitatively superior compared to anti-PD-1 in the same tumors. Finally, CD8-IL2 also induced functional T cell reinvigoration in tumors that are resistant to PD-1 blockade, suggesting the presence of a tumor-specific T cell pool that either cannot be reinvigorated by PD-1 blockade alone or is distinct from the one susceptible to reprogramming by PD-1 blockade.

Results

CD8-IL2 induces specific and potent $CD8^+$ T cell activation in human tumor tissue

$CD8^+$ T cells are key effectors of antitumor immunity[3,34,35], and strategies that offer the possibility to specifically boost the function of antigen-activated $CD8^+$ T cells are thus of value. We here explored a novel IL2 mutein cis-targeted to the CD8β chain (CD8-IL2, also called AB248) allowing the selective delivery of an immunostimulatory IL2 signal to $CD8^+$ T cells. To avoid T_{reg} expansion and antigen-independent T cell activation, CD8-IL2 was designed to contain an IL2 mutein with no detectable IL2Rα binding and reduced binding to the signaling IL2Rβγ complex[32]. To evaluate the specificity of the molecule, we stimulated single-cell digests of human tumors with different concentrations of either CD8-IL2, human recombinant IL2 (hrIL2), or an untargeted not-alpha IL2 variant (IL2v). Assessing the induction of the proliferation marker Ki67 as a direct IL2 effect, we observed that, whereas both IL2v and hrIL2 induced Ki67 expression in tumor-infiltrating T_{regs} and conventional $CD4^+$ T (T_{conv}) cells, CD8-IL2 did not activate these cell types, even at the highest concentration tested (**Fig. S1a**). Moreover, CD8-IL2 induced Ki67 expression in $CD8^+$ T cells at 1,000-fold lower concentrations as compared to hrIL2 and IL2v, demonstrating its potency. Analysis of T cell expansion over five days confirmed that T_{regs} expanded significantly less following CD8-IL2 treatment as compared to IL2v treatment (**Fig. S1b**). Interestingly, T_{regs} in human tumors not only expressed high levels of the IL2Rα-subunit, but also of the β-subunit relative to $CD8^+$ T cells (**Fig. S1c**), providing a further incentive for CD8-targeting to achieve $CD8^+$ T cell specificity.

Next, we aimed to address the potential of CD8-IL2 to reinvigorate tumor-infiltrating $CD8^+$ T cells in their native tissue context, using a recently developed PDTF platform[10,33]. PDTFs are

3D fragments of human tumor tissue preserving the TME contexture outside of the patient and allowing short-term ex vivo culture in the absence or presence of immunotherapies. Of note, PDTFs display immune activation upon ex vivo PD-1 blockade that is highly correlated with the clinical response of the patient to the same treatment[10], underlining the relevance of such early immune activation in situ. To examine the effect of selective delivery of IL2 to $CD8^+$ T cells on intratumoral T cell activity, PDTFs from 23 human tumors were cultured in the absence or presence of CD8-IL2 for 48 hrs. (**Fig. 1a**). The PDTFs analyzed comprised five different cancer types, renal cell carcinoma (RE), ovarian carcinoma (OV), melanoma (MEL), non-small cell lung cancer (LU), and breast cancer (BR), and were enriched for immune-infiltrated tumors (**Fig. S1d-e**, **Table S1**). Ex vivo treatment with CD8-IL2 induced markers associated with cytotoxicity (Granzyme B), proliferation (Ki67), and activation (PD-1, CD137) in $CD8^+$ T cells in the vast majority of tumors (**Fig. 1b,c**, **Fig. S2**). In contrast, stimulation with anti-CD8β alone did not induce any of the observed changes (**Fig. S3a**). Notably, CD8-IL2 also increased IFNγ production in $CD8^+$ T cells (**Fig. 1d**), suggesting their functional reinvigoration.

The CD8-targeted IL2 mutein used here binds to the IL2Rβ/γ subunits, which also form a receptor for IL15. As similarities in IL2 and IL15 signaling have been observed[36], we compared the effects of CD8-IL2 and IL15 in PDTFs. As expected, we observed similar activation of $CD8^+$ T cells upon both stimulations (**Fig. S3b**). However, IL15 also strongly activated NK cells (**Fig. S3c**), which can mediate toxicity but are dispensable for anti-tumor activity[14,37,38], highlighting the value of directing cytokines towards specific cell types.

Intratumoral T cells can acquire diverse phenotypes, and particularly dysfunctional T cells form a gradient of states, ranging from dysfunctional precursor cells with capacity for self-renewal to terminally differentiated late dysfunctional T cells[39-41]. Recent reports in murine models described that IL2 molecules that are cis-targeted to $PD\text{-}1^+$ T cells[16,42] or that are provided in combination with PD-1 blockade[15] may mainly drive the differentiation of early dysfunctional T cells into functional effectors. To understand to what extent this observation would translate to human tumors, we analyzed the effects of CD8-IL2 on $CD8^+$ T cells with distinct differentiation states. Using CD39 as a marker to differentiate $CD8^+$ T cells with early ($PD\text{-}1^+CD39^-$) and late ($PD\text{-}1^+CD39^+$) dysfunction (**Fig. 1e**), we observed that CD8-IL2 increased Granzyme B and Ki67 expression in both subsets. Conversely, CD137 was mainly increased in $PD\text{-}1^+CD39^+$ T cells, suggesting differences in the reinvigoration of the early and late dysfunctional T cell pools (**Fig. 1f**). Supporting this notion, only $PD\text{-}1^+CD39^+$ T cells showed increased degranulation after 6 hrs. of CD8-IL2 treatment (**Fig. S3d**), suggesting that despite the increase in Granzyme B expression in both subsets, only late dysfunctional T cells may acquire cytolytic immune function.

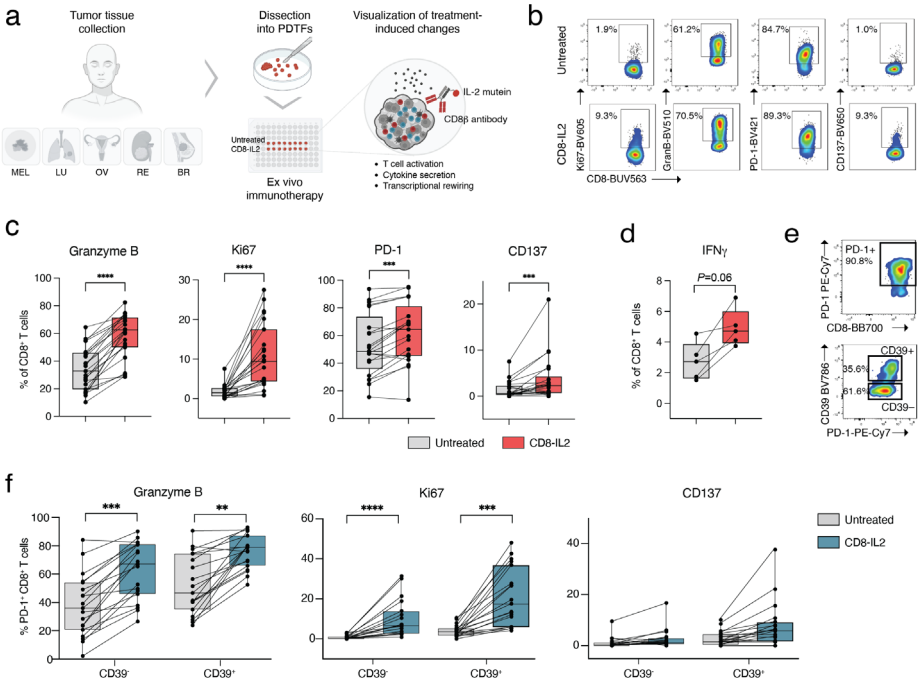

Figure 1. CD8-IL2 selectively and potently activates CD8⁺ T cells in human tumor fragments. (a) Overview of the patient-derived tumor fragment (PDTF) platform and analysis strategy (created with BioRender.com). **(b)** Representative flow cytometry plots displaying markers of proliferation (Ki67), cytotoxicity (Granzyme B), and activation (PD-1, CD137) in intratumoral CD8⁺ T cells from PDTFs that were left untreated or treated with ex vivo CD8-IL2 (RE098). **(c)** Quantification of activation markers on total intratumoral CD8⁺ T cells in untreated or CD8-IL2-treated PDTFs measured by flow cytometry (n=23). **(d)** Quantification of intracellular IFNγ in total intratumoral CD8⁺ T cells in untreated or CD8-IL2-treated tumor digests measured by flow cytometry (n=5). **(e)** Representative gating for PD-1⁺CD39⁺ (late dysfunctional) and PD-1⁺CD39⁻ (early dysfunctional cells) CD8⁺ T cells. **(f)** Same analysis as in (c) but separated for PD-1⁺CD39⁺ (late dysfunctional) and PD-1⁺CD39⁻ (early dysfunctional cells). ****$P < 0.0001$, ***$P < 0.001$, **$P < 0.01$ by two-tailed Wilcoxon test (c, d). ***$P < 0.001$, **$P < 0.01$ by Friedman test corrected for multiple comparisons (f). Only significant comparisons are shown.

Given that T cells upregulate PD-1 on their surface after antigen encounter, previous studies have explored PD-1 cis-targeting of IL2 for the selective activation of the antigen-activated T cell pool[16,42]. In our dataset, on average 80% of CD8⁺ T cells also expressed PD-1, suggesting that most of the cells would be targeted by both approaches (**Fig. S3e**). In contrast, only half of the PD-1⁺ T cells were CD8⁺, suggesting that PD-1-targeted compounds may also exert effects on other cells including T_{regs} (**Fig. S3f**). As a comparison, CD8b-expressing cells were almost exclusively CD3⁺ T cells (**Fig. S3g**). To directly compare IL2 targeting to either CD8 or PD-1, we treated PDTFs from seven tumors with CD8-IL2 or an IL2v fused to PD-1 (PD1-IL2). Both CD8-IL2 and PD1-IL2 induced Ki67 expression in CD8⁺ T cells, however PD1-IL2 showed a lower effect in 5/8 tumors (**Fig. S3h**). To understand

whether similar CD8$^+$ T cell populations are activated, we compared the phenotype of Ki67$^+$ and Ki67$^-$ cells following both treatments. We found that CD8-IL2 and PD1-IL2 similarly induced proliferation of CD8$^+$ T cells expressing CD39 and CD103 (**Fig. S3i**), indicating that both targeting strategies activate a subset that is likely to be tumor-reactivity[43,44]. In line with the observed PD-1 expression by intratumoral T_{regs}, we saw an increase in this subset following ex vivo PD1-IL2 but not CD8-IL2 treatment (**Fig. S3h**). Jointly, these data suggest that CD8-IL2 and PD1-IL2 treatments are comparable in their effects on CD8$^+$ T cells in human tumor tissue, but PD1-IL2 treatment may result in a higher fraction of T_{regs}, potentially limiting antitumor immunity.

Immune reactivation upon CD8-IL2 depends on concomitant TCR signaling

We previously found that immune reactivation, here defined by the induction of pro-inflammatory cytokines and chemokines, in PDTFs is a strong predictor of clinical response to anti-PD-1[10]. Therefore, we next assessed whether intratumoral T cell activation by CD8-IL2 translated into such a functional cytokine response. Ex vivo CD8-IL2 treatment induced production of multiple soluble mediators including Granzyme B, TNFα, IFNγ or its downstream chemokines in part of the tumors (**Fig. 2a**). To distinguish tumors with or without such a CD8-IL2-induced immunological response, we quantified the overall change in soluble mediator activity by cumulating the normalized delta values between the treated and untreated condition for each parameter. Based on this analysis, tumors were segregated into CD8-IL2 responders (CD8-IL2-R, 13/23) and CD8-IL2 non-responders (CD8-IL2-NR, 10/23), distinguished by high and low cumulative scores, respectively (**Fig. 2a-c**). To delineate the mechanisms underlying the heterogeneity in immunological reinvigoration, we next explored whether CD8-IL2-R and -NR tumors differed in baseline tumor properties or the extent and quality of T cell activation. Profiling the TME composition of each tumor by flow cytometry revealed that, with exception of CD4$^+$ T cells, the main immune populations were not substantially different between responding and non-responding groups (**Fig. S4a**). CD8-IL2-R tumors contained significantly less CD4$^+$ T_{conv} cells in favor of more T_{regs}, i.e. of a CD39$^+$ subset associated with high suppressive capacity[45,46]. We did not observe any difference in IL2Rβ/γ-expression on CD8$^+$ T cells, and PD-L1 expression on myeloid and tumor cells, respectively. MHC class I expression on cancer cells was higher in CD8-IL2-R, though without reaching statistical significance (**Fig. S4a**). Based on our observation that CD8$^+$ T cells proliferating upon CD8-IL2 expressed a dysfunctional profile, we assessed the baseline frequency of dysfunctional (PD-1$^+$CD39$^+$CD103$^+$) and memory (PD-1$^+$IL7R$^+$) T cell populations. The CD8$^+$ compartment in responding tumors harbored significantly more dysfunctional cells as compared to non-responding tumors, which conversely were enriched for memory T cells (**Fig. 2d**). CD8$^+$ T cells in responding tumors also showed higher production of CXCL13 (**Fig. 2d**), another property associated with tumor reactivity[47-49].

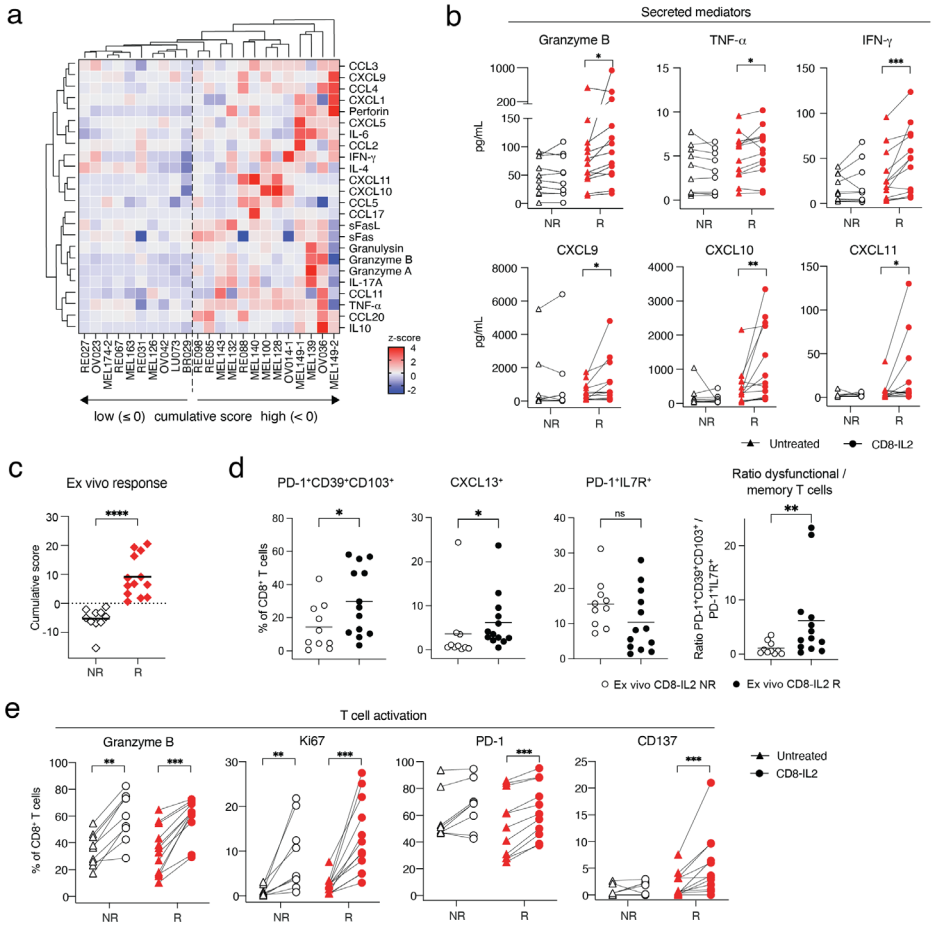

Figure 2. CD8-IL2 induces immunological responses in a subset of tumors. (a) Heatmap displaying normalized delta values (CD8-IL2 condition – untreated condition) of 24 soluble mediators secreted by PDTFs, ordered according to unsupervised hierarchical clustering (n=23). **(b)** Examples of T cell effector cytokines (IFNγ, TNFα), cytotoxic mediators (Granzyme B), and chemokines (CXCL9, CXCL10, and CXCL11) in unstimulated and CD8-IL2 stimulated PDTFs in ex vivo responding (R) and non-responding (NR) tumors. **(c)** Separation of tumors by cumulative z-scores of soluble mediators in CD8-IL2 R and NR tumors. **(d)** Baseline infiltration of dysfunctional ($PD\text{-}1^{+}CD39^{+}CD103^{+}$) and memory ($PD\text{-}1^{+}IL\text{-}7R^{+}$) $CD8^{+}$ T cells and CXCL13 expression in CD8-IL2-R and NR tumors measured by flow cytometry. **(e)** $CD8^{+}$ T cell activation markers measured by flow cytometry separately plotted for R and NR tumors. $^{****}P < 0.0001$, $^{***}P < 0.001$, $^{**}P < 0.01$, $^{*}P < 0.05$ by two-tailed Wilcoxon test (b-e). Only significant comparisons are shown.

Altogether, these data suggest distinct $CD8^{+}$ T cell landscapes in CD8-IL2-R and NR tumors. Thus, we next aimed to understand whether immunological response to CD8-IL2 associates with qualitative differences in T cell activation. Surprisingly, Ki67 and Granzyme B expression were increased in both CD8-IL2-R and -NR upon treatment,

suggesting comparable acquisition of markers associated with effector capacity and proliferation independent of cytokine production in the TME. By contrast, the induction of PD-1 and particularly CD137 expression was largely restricted to the CD8-IL2-R group (**Fig. 2e**). Notably, CD8-IL2-R tumors already displayed higher CD137 and Ki67 expression at baseline (**Fig. S4b**), compatible with ongoing tumor recognition in those tumors. This also corresponded with higher basal cytokine production in these samples (**Fig. S4c**), suggesting that CD8-IL2 may reinvigorate a pre-existing anti-tumor response. Based on these observations and since CD137 is upregulated shortly after TCR triggering[50], we hypothesized that simultaneous antigen recognition is required for cytokine responses to ex vivo CD8-IL2, but not for the induction of effector capacity. To test this, we pretreated eight CD8-IL2-R tumors with an Lck inhibitor (LCKi), which stalls signaling directly downstream of the TCR (**Fig. 3a**). Remarkably, Lck inhibition before CD8-IL2 treatment resulted in a significant decrease, and in some cases complete abolition, of cytokine and chemokine secretion, also evidenced by a marked reduction in the cumulative score (**Fig. 3b-d, Fig. S4d**). Consistent with antigen recognition being essential for these responses, $CD8^+$ T cells did not upregulate CD137 when TCR signaling was blocked before CD8-IL2 treatment. Strikingly, Granzyme B, PD-1, and Ki67 expression still increased despite the absence of TCR signaling (**Fig. 3e**). Similar observations were made when an MHC class I-blocking antibody was used instead of Lck inhibition (**Fig. S4e**). These data imply that CD8-IL2 may induce effector capacity in T cells independent of them receiving a TCR signal, but that effector function occurs only in the presence of the latter. To test this hypothesis in a model in which the presence of a TCR stimulus can be experimentally controlled, we stimulated human PBMCs with CD8-IL2 and increasing concentrations of anti-CD3. In line with our observations in PDTFs, CD8-IL2 treatment alone was able to induce intracellular Granzyme B expression, implying that IL2 signaling is sufficient to promote T cell effector capacity (**Fig. 3f**). Addition of CD8-IL2 to *anti*-CD3 stimulation further increased Granzyme B expression compared to *anti*-CD3 alone in a dose-dependent manner. In contrast, extracellular release of Granzyme B was not induced by CD8-IL2 alone, but by anti-CD3 stimulation, and was further boosted when CD8-IL2 and anti-CD3 were combined (**Fig. 3g**). Similar effects were observed for IFNg secretion, representing another important effector function of $CD8^+$ T cells (**Fig. 3g**). Jointly, these results are compatible with a model, in which CD8-IL2 broadly induces effector capacity in intratumoral $CD8^+$ T cells, but restores effect function only in the presence of simultaneous antigen recognition.

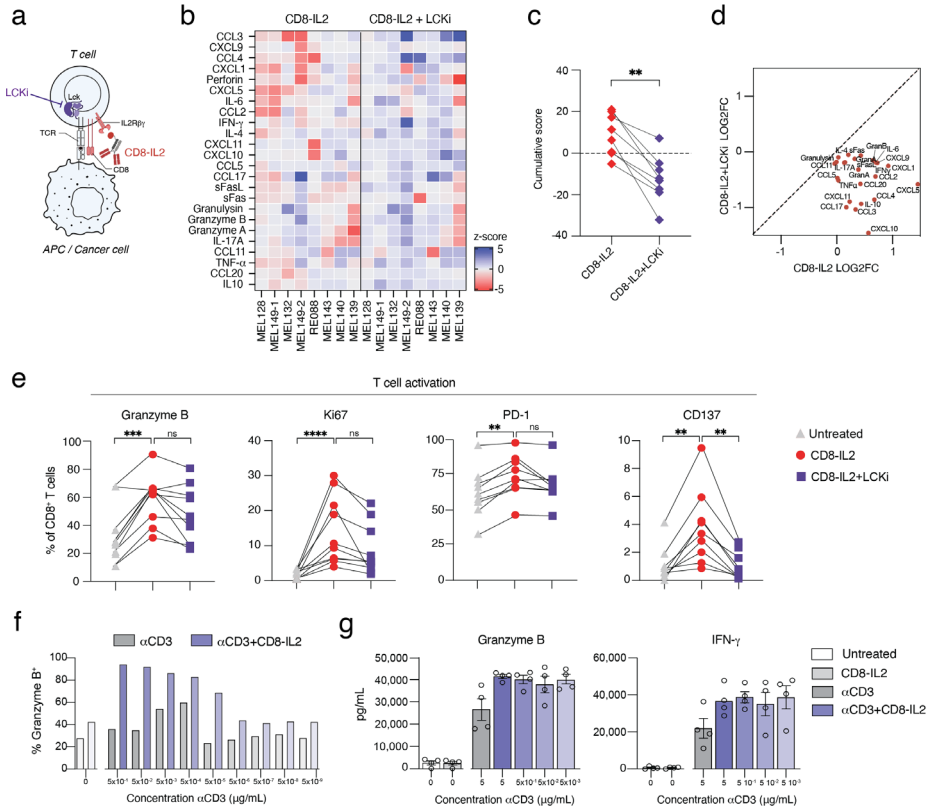

Figure 3. TCR signaling is required for a functional immune response to CD8-IL2. (a) Schematic overview of Lck inhibition (LCKi) in the context of CD8-IL2 treatment (created with BioRender.com). **(b)** Normalized delta values (CD8-IL2 or CD8-IL2+LCKi condition – untreated condition) of soluble mediators secreted by PDTFs. Tumor samples were selected based on prior response to CD8-IL2 (as shown in Fig. 2a) and material availability (n=8). **(c)** Cumulative z-scores of soluble mediators in CD8-IL2-responding tumors when treated with either CD8-IL2 or CD8-IL2+LCKi. **(d)** Correlation of log2 fold changes (LOG2FC) of soluble mediators induced by either CD8-IL2 and CD8-IL2+LCKi versus the untreated condition. **(e)** Intratumoral CD8⁺ T cell activation of CD8-IL2-responding tumors upon CD8-IL2 and CD8-IL2+LCKi treatment measured by flow cytometry. **(f)** Intracellular expression of Granzyme B and **(g)** secreted soluble Granzyme B and IFNγ in human PBMCs upon 5-day incubation with decreasing concentrations of anti-CD3 in the absence and presence of CD8-IL2 (n=4). $^{**}P < 0.01$ by two-tailed Mann-Whitney *U* test (c). $^{****}P < 0.0001$, $^{***}P < 0.001$, $^{**}P < 0.01$ by Friedman test corrected for multiple comparisons (e).

CD8-IL2 induces profound transcriptional rewiring of the intratumoral T cell landscape

To understand how CD8-IL2 treatment reactivates intratumoral CD8⁺ T cells, we performed single-cell RNA and TCR sequencing (scRNA&TCRseq) of PDTFs in the absence or presence of CD8-IL2. To benchmark the observed alterations, we cultured additional fragments from the same tumors with a number of other stimulations including CD8-IL2+LCKi, IL2v,

anti-PD-1, anti-PD-1+CD8-IL2, anti-CD3 and anti-CD3+CD8-IL2. Our cohort included five tumors (RE, *N*=2; OV, *N*=1; MEL, *N*=2) with distinct immunological responses to CD8-IL2 and anti-PD-1, respectively, based on previous experiments (**Fig. 2a**, **Fig. S5a**). Comparable immune cell numbers were isolated and sequenced for each treatment condition per tumor (**Fig. S5b**). Clustering analysis distinguished the main immune cell populations, including $CD4^+$ T cells, $CD8^+$ T cells, B cells, γδ T cells and NK cells, which were consistently identified across all tumors and conditions (**Fig. S5c-f**). As CD8-IL2 exclusively activates $CD8^+$ T cells, we focused our further analysis on this subset. Treatment conditions containing anti-CD3 stimulation were not included in the subsequent analysis but kept as an independent reference for TCR-induced activation (see below). Clustering of the intratumoral $CD8^+$ T cell pool from the remaining conditions yielded data on 8,712 cells. As patient-specific clusters were observed, data integration was performed leading to a more homogenous representation of clusters across patients without overcorrection of sample expression profiles (**Fig. S6a,b**). Next, we performed a more detailed characterization of the distinct $CD8^+$ T cell clusters. To this end, clusters were annotated using differential gene expression analysis, revealing 13 distinct $CD8^+$ states including naïve-like (Naïve_c1_BNIP, Naïve_c2_RP), memory (Mem_c1_IL7R, Mem_c2_CAPG), transitional (Trans_KLRG1), dysfunctional (Dys_c1_TOX, Dys_c2_HLA-DRB1), cycling (Cycl_c1, Cycl_c2, Cycl_c3), effector (Eff_FCGR3A), NK-like (NK-like_KLRC1), and IFNγ-sensing (IFN_ISG15) clusters (**Fig. 4a**, **Fig. S6c**). These annotations were further validated by overlaying previously described gene expression signatures for effector[51], memory[51], exhausted[52], and proliferating[53] states on the UMAP (**Fig. 4b**). We next assessed canonical $CD8^+$ T cell markers previously described in scRNA-seq studies of human intratumoral T cells[54] to further characterize the distinct clusters (**Fig. 4c**). The Mem_c1_IL7R and Mem_c2_CAPG states showed similar expression of T cell memory markers, however the Mem_c2_CAPG cluster also expressed genes associated with cytotoxicity and effector differentiation (*GZMA*, *GZMB*, *PRF1*, *CXCR3*), suggesting that it may represent a more activated state of Mem_c1. Similar patterns were observed in the two dysfunctional clusters, with Dys_c2_HLA-DRB1 displaying a highly activated state as compared to Dys_c1_TOX, with increased expression of granzyme gene family members, *IFNG*, *TNFRSF9*, *TNFRSF18*, and *HLA class II genes*. The Trans_KLRG1 cluster expressed low levels of inhibitory receptors and effector molecules and was positive for *TCF7*, in line with a more precursor-like state. Interestingly, the three cycling clusters showed distinct profiles, with Cycl_c2 displaying a more memory-like phenotype and lower expression of dysfunction markers as compared to Cycl_c1 and Cycl_c3. Moreover, Cycl_c3 contained mostly cells in the G2M phase of the cell cycle, in contrast to Cycl_c1 and Cycl_c2 which corresponded to the S phase (**Fig. S6d**).

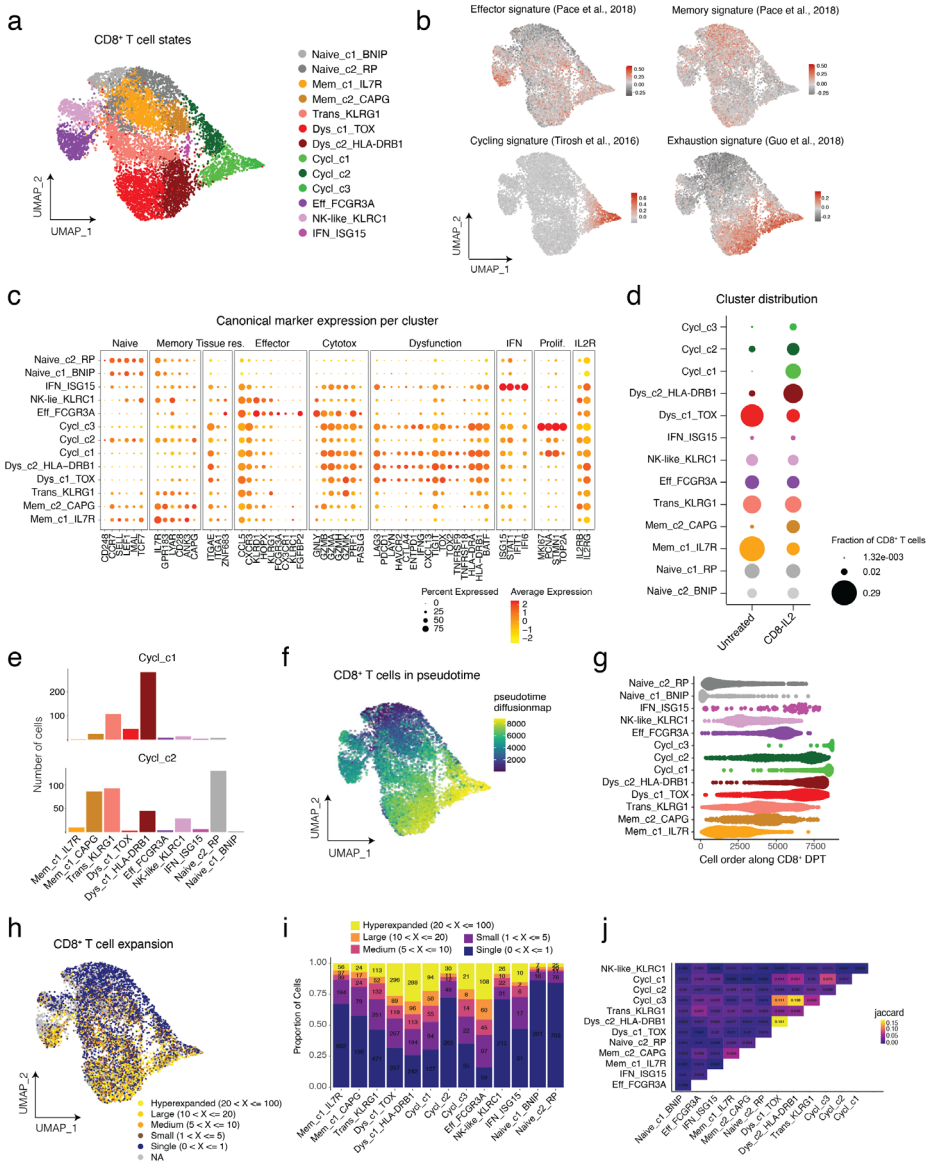

Figure 4. CD8-IL2 elicits broad transcriptional rewiring of the intratumoral CD8⁺ T cell landscape. (a) UMAP visualization of all intratumoral CD8⁺ T cells (from untreated and all treated conditions) in human tumor fragments from five tumors (n=8,712 cells) identifying 13 different clusters. **(b)** Normalized expression of a selected set of previously published gene signatures for effector cells[51], memory cells[51], cycling cells[53] and T cell exhaustion[52]. **(c)** Annotated canonical marker gene expression in the different CD8⁺ T cell clusters. **(d)** Cluster fractions of CD8⁺ T cell states derived from untreated or CD8-IL2 treated PDTFs. **(e)** Quantification of the distribution of the number of cells label transferred from the Cycl_c1 and Cycl_c2 clusters into the rest of the cell populations. (This analysis was not performed for the Cycl_c3 cluster due to limited cell numbers). **(f)** UMAP visualization of CD8⁺ T displaying the cells in diffusion pseudotime (DPT). **(g)** Cell order along DPT

for each CD8⁺ T cell cluster. **(h)** UMAP visualization of the T cell clonal size and **(i)** per CD8⁺ T cell cluster. Clonotypes are ranked based on frequency ranges: 'single' = found in 1 cell, 'small' = in >1 and <5 cells, 'medium' = in >5 and <10 cells, 'large' = >10 and <20 cells, 'hyperexpanded' = in >20 and <100 cells. **(j)** Clonal overlap between CD8⁺ T cell clusters calculated by Jaccard index.

To understand how the identified cell states relate to treatment, we first compared cluster distribution between untreated and CD8-IL2-treated PDTF conditions (**Fig. 4d, Fig. S7a**). Notably, five clusters newly formed or substantially increased upon CD8-IL2, comprising all three cycling clusters (Cycl_c1, Cycl_c2, Cycl_c3), as well as the activated Mem_c2_CAPG and Dys_c2_HLA-DRB1 clusters. Conversely, the Mem_c1_IL7R and Dys_c1_TOX clusters decreased, suggesting that CD8-IL2 treatment may trigger the transcriptional reconfiguration of CD8⁺ T cells shifting them towards more activated states. Underscoring this notion, we found that the newly formed states upon CD8-IL2, including the dysfunctional cluster, showed increased expression of a transcriptional signature derived from effector T cells generated during acute infection[53] (**Fig. S7b,c**). We next compared the CD8-IL2-induced changes to those elicited by an IL2v lacking the CD8-targeting moiety. At same concentrations, IL2v induced minimal shifts in clusters compared to CD8-IL2 (**Fig. S7d**), in line with our flow data (**Fig. S1a**) and prior reports that untargeted IL2Rbg agonists fail to induce better effector cells[42].

As a next question, we aimed to identify from which cell states the CD8-IL2-induced clusters originate. Therefore, we first conducted label transfer analysis of the proliferating Cycl_c1 and Cycl_c2 clusters (Cycl_c3 contained too limited cell numbers for this analysis) (**Fig. 4e**). This revealed that cells from Cycl_c1 were mainly derived from dysfunctional and transitional states, with Dys_c2_HLA-DRB1 contributing most, whereas Cycl_c2 comprised multiple cell states including naïve, transitional, dysfunctional, memory, and NK-like states. As an alternative approach to reconstruct developmental relationships between the clusters, we performed diffusion pseudotime (DPT) analysis[55]. Ordering the clusters along DPT revealed that naïve clusters were early in pseudotime, followed by memory, transitional, and dysfunctional states, consistent with the dysfunctional differentiation gradient of CD8⁺ T cells in the TME (**Fig. 4f,g**). The effector and NK-like states were situated between the naïve-like and dysfunctional states and appeared to form a separate trajectory. The IFN_ISG15 cluster, likely formed by cells responding to the secreted IFNγ, appeared later in pseudotime. In line with their treatment-induced differentiation, the Mem_c2_CAPG and Dys_c2_HLA-DRB1 clusters were later in DPT than their matched Mem_c1_IL7R and Dys_c1_TOX states that were predominant in untreated samples. Notably, the three cycling clusters exhibited differences in pseudotime, with Cycl_c2 appearing earlier and more spread over DPT compared to the other two cycling clusters, supportive of distinct trajectories as suggested by the label transfer analysis.

To further corroborate these findings, we parsed the TCR-seq data to connect clonal information with the individual cellular phenotypes. TCR clonal expansion per cluster was lowest in the naïve clusters, increased slightly in memory and transitional clusters,

and reached the highest level in the effector and dysfunctional states (**Fig. 4h,i**), consistent with prior studies and potential tumor recognition by these clones[57-59]. Again, we observed distinct expansion patterns among the cycling clusters, with a high fraction of expanded clones in Cycl_c1 and Cycl_c3, and lower TCR expansion in Cycl_c2, in line with the origin of the latter from multiple clonally diverse cell states. To further probe relationships between clusters, we next determined clonal overlap between the CD8$^+$ states (**Fig. 4j**). Focusing on the five cell states emerging upon CD8-IL2, we observed low-level TCR sharing of Mem_c2_CAPG and Cycl_c2 with the Mem_c1_IL7R and Trans_KLRG1 clusters. By contrast, Dys_c2_HLA-DRB1, Cycl_c1, and Cycl_c3 states showed substantial clonal overlap among themselves, with Dys_c1_TOX, and to a lesser extent with the Trans_KLRG1 cluster, suggesting a separate differentiation trajectory induced within the dysfunctional axis.

CD8-IL2 induces TCR-dependent reactivation of the tumor-specific dysfunctional T cell pool

Taken together, the above observations are compatible with the model suggested by our flow analyses, in which CD8-IL2 can broadly activate tumor-infiltrating CD8$^+$ T cells, but may induce distinct rewiring of tumor-specific T cells that also receive a TCR stimulus. To connect the single-cell data to our earlier flow experiments, we overlayed transcript levels of *TNFRSF9* (CD137), *MKI67* (Ki67), *GZMB* (Granzyme B), and *IFNG* (IFNγ) on the UMAP (**Fig. 5a**). Expression of these transcripts enriched mostly in cluster areas induced upon CD8-IL2 treatment but not in those already present in unstimulated samples, in line with CD8-IL2-induced effector capacity. *MKI67* expression was logically restricted to the cycling clusters. Of note, we found distinct expression patterns of *GZMB, TNFRSF9* and *IFNG* between the activated clusters. In agreement with our earlier protein data, *GZMB* was highly expressed in all induced clusters, whereas *IFNG* and especially *TNFRSF9* expression was more concentrated in cells of the dysfunctional axis, compatible with the latter also receiving TCR-dependent signals.

To visualize changes in distribution of the most expanded TCRs upon treatment, we performed clonal overlay analysis on the cell states derived from untreated and CD8-IL2-treated PDTFs (**Fig. S7e**). In the untreated condition, the most expanded TCRs were present in the Dys_c1_TOX cluster, whereas upon CD8-IL2 treatment they enriched in the Dys_c2_HLA-DRB1, Cycl_c1, and Cycl_c3 clusters, supporting the notion that the activation observed in these clusters is dependent on IL2R stimulation in the context of TCR triggering. To test this hypothesis, we compared the effects of CD8-IL2 to a CD8-IL2+LCKi condition tested in the same tumors (**Fig. S5a**). DPT analysis of CD8$^+$ T cells from the untreated, CD8-IL2, and CD8-IL2+LCKi conditions revealed that TCR blockade decreased the overall progression of cells in pseudotime, implying that they were unable to undergo full activation and differentiation without receiving a TCR stimulus (**Fig. S7f**). Plotting the cell densities from those conditions on the UMAP illustrated that CD8-IL2 still induced new cell states even when TCR signaling was blocked (**Fig. 5b**). Specifically, the Mem_c2_CAPG and Cycl_c2 clusters appeared to be induced largely independent of TCR signaling, whereas

the formation of Dys_c2_HLA-DRB1, Cycl_c1 and Cycl_c3 showed varying dependence on TCR triggering (**Fig. 5c**). The remaining clusters were mostly unaffected by TCR blockade (**Fig. S7g**). To further probe the influence of IL2R and TCR signals on these clusters, we performed label transfer of cell states from the CD8-IL2 condition on CD8⁺ T cells from anti-CD3- or anti-CD3+CD8-IL2-treated PDTFs, a setting in which all T cells equally receive a TCR stimulus (note that these conditions were excluded from the clustering). Upon anti-CD3 stimulation, a small fraction of CD8⁺ T cells acquired the activated Dys_c2_HLA-DRB1 or Cycl_c1 states while the Mem_c2_CAPG and Cycl_c2 clusters were only marginally induced, confirming the latter states' dependency on IL2. In contrast, all five activated cell states emerged upon anti-CD3+CD8-IL2 encompassing >70% of CD8⁺ T cells in this condition (**Fig. S7h**), indicating that at least part of these states require both IL2 and TCR signals.

To understand which of these CD8⁺ states have tumor recognition capacity, we sorted dysfunctional, memory-like, effector-like, and transitional subsets from four tumor samples based on key transcriptional markers (**Fig. 5d,e**). The respective cell states of the sorted subsets were confirmed by another scRNAseq experiment (**Fig. S8a**). Moreover, we validated that the subsets identified by these markers recapitulate the distinct patterns of CD137 and Granzyme B expression in dysfunctional compared to other cell states upon CD8-IL2 (**Fig. S8b**). We next expanded the different subsets and co-cultured them with autologous tumor digest with or without CD8-IL2 (**Fig. 5f, Fig. S8c,d**). In line with clonal expansion patterns, tumor recognition, as measured by CD137 expression, degranulation and IFNγ/TNFα production, was largely restricted to the dysfunctional subsets in all four tumors with exception of one tumor in which also T cells expanded from transitional cells showed reactivity (OV054-1). Addition of CD8-IL2 to the co-cultures did not increase degranulation or cytokine production, as these cells probably already acquired maximal effector capacity during expansion in high-dose IL2. Of note, CD8-IL2 still increased the expression of CD137 in dysfunctional and transitional T cells upon tumor recognition (**Fig. 5g**), suggesting an additional effect via enhancing TCR signaling. Altogether, these data confirm that tumor reactivity is mostly restricted to T cells with dysfunctional phenotypes, and suggest a mechanism in which CD8-IL2 may promote reinvigoration both via TCR-dependent and -independent signals.

CD8⁺ T cells acquire distinct TCR-dependent and -independent gene programs following CD8-IL2 treatment

To further uncouple the effects induced by either IL2R- or TCR-signaling, we devised two specific gene programs (**Fig. S9a, Supplementary Data 1**). Reasoning that T cells exposed to CD8-IL2 in the presence of Lck inhibition should only receive IL2 and no TCR signals, we constructed an IL2 program based on differential gene expression (DGE) analysis between the untreated and CD8-IL2+LCKi conditions (**Fig. S9b**). Similarly, a TCR program was developed based on DGE between cells from PDTFs that were either untreated or stimulated by anti-CD3 (**Fig. S9c**).

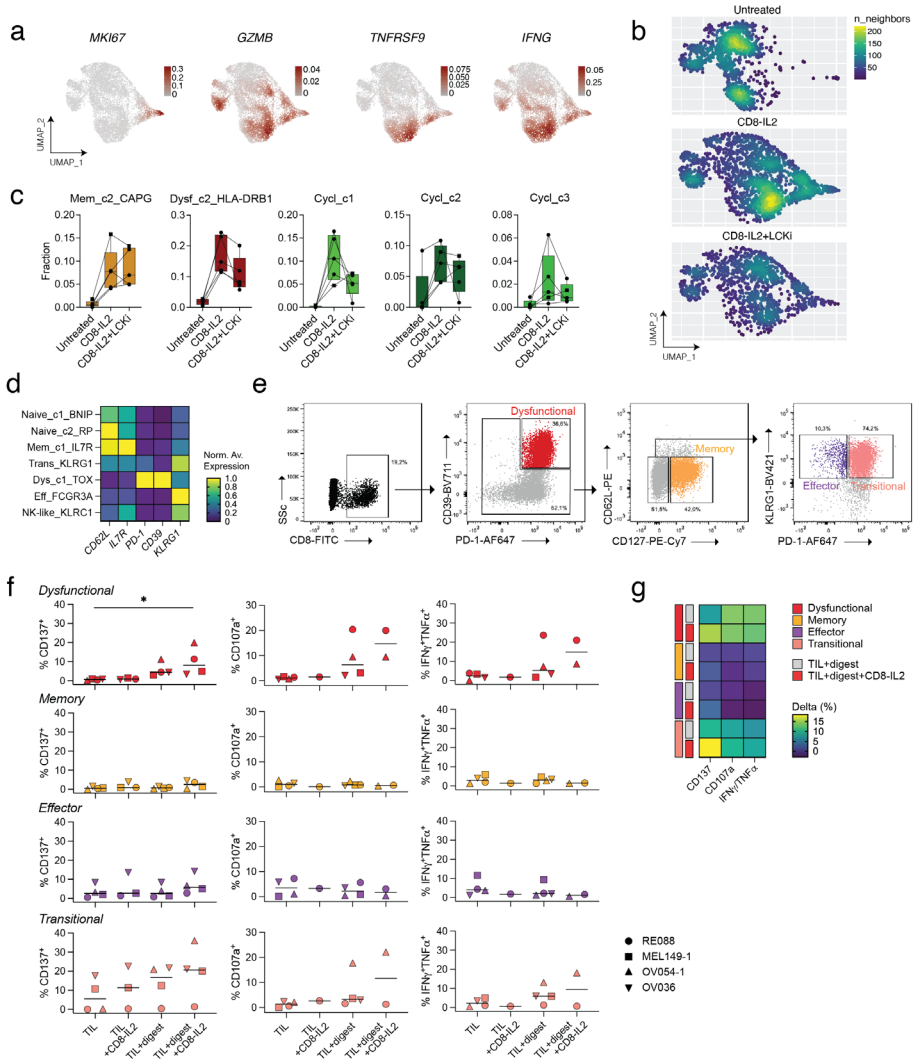

Figure 5. CD8-IL2 activates the dysfunctional tumor-specific CD8⁺ T cell pool. (a) UMAPs of intratumoral CD8⁺ T cells displaying expression of *MKI67*, *GZMB*, *TNFRSF9* and *IFNG* (n=5 tumors). **(b)** UMAP representation of CD8⁺ T cell density in the untreated, CD8-IL2-treated, and CD8-IL2+LCKi conditions. **(c)** Paired fractions of CD8⁺ T cell clusters in untreated, CD8-IL2-treated, and CD8-IL2+LCKi conditions for the five clusters that increased or formed in response to CD8-IL2 treatment. The one CD8-IL2-NR tumors (RE027) is marked by a square, the four responders are depicted as circles. **(d)** Heatmap displaying normalized expression of genes discriminating the distinct transcriptional CD8⁺ T cell states present in untreated PDTFs. **(e)** Gating strategy for flow cytometric sorting of dysfunctional, memory, effector, and transitional CD8⁺ T cells. **(f)** Tumor reactivity co-culture of expanded TILs from sorted dysfunctional, memory, effector, and transitional CD8⁺ T cells with autologous tumor digest in the presence or absence of CD8-IL2. Reactivity was measured by assessing CD137, CD107α and IFNγ/TNFα expression by flow cytometry. Note that due to differences in expansion, not all populations reached sufficient cell numbers for all experiments. *$P < 0.05$ by Kruskal-Wallis test. **(g)** Heatmap showing the difference in marker expression between TIL+digest or TIL+digest+CD8-IL2 versus TIL alone as measured in **(f)**. Values are averaged for each marker between the two tumors for which data for all conditions were available (RE088, OV054-1).

First, we assessed the expression of the two programs across conditions. Notably, the IL2 program was increased in both the CD8-IL2 and CD8-IL2+LCKi conditions, while the TCR program was specifically enriched following CD8-IL2 and not when the LCKi was co-administered (**Fig. 6a**). Vice versa, the increase in the IL2 program upon anti-CD3 stimulation was only marginal, implying that TCR-signaling alone is not sufficient for its induction (**Fig. S9d**). Interestingly, adding CD8-IL2 to anti-CD3 further increased the expression of the TCR program (**Fig. S9d**), supporting the notion that IL2 may enhance TCR-mediated signals.

Overlaying both signatures on the UMAP confirmed that the IL2 program was broadly induced across cell states upon CD8-IL2 treatment, whereas the induction of the TCR program was restricted to the dysfunctional axis (**Fig. 6b**), aligning with the previously observed tumor reactivity patterns. DPT analysis of the two gene programs indicated that the IL2 program continuously increased with pseudotime, compatible with the CD8-IL2-induced clusters arising later in pseudotime (**Fig. 6c**). Notably, the increase of the IL2 program over pseudotime was unaffected by TCR blockade. In contrast, the TCR program was only acquired by fully differentiated cells at the end of pseudotime, and was abolished upon blockade of TCR-signaling. Assessing the gene programs across clusters, we found –in line with tumor reactivity patterns– that the IL2 program was active in all CD8-IL2-induced clusters, whereas the TCR program was mostly confined to the dysfunctional, Cycl_c1 and Cycl_c3 clusters (**Fig. 6d,e**). Interestingly, corresponding with the protein expression data, the TCR program was to some extent already detectable in untreated samples particularly in the Dys_c1_TOX cluster (**Fig. 6c-e**), implying ongoing TCR recognition in dysfunctional T cells that likely translates into functional immune reactivation upon reinvigoration by CD8-IL2.

In recent work, antigen-specific $CD8^+$ T cells in murine cancer and chronic infection models have been found to acquire a 'better effector' state after PD-1-targeted IL2 treatment[42]. Comparison of this 'better effector' state to the IL2 and TCR programs showed that the 'better effector' signature slightly increased in the activated memory and dysfunctional states that emerged upon CD8-IL2 treatment, but not in the cycling clusters (**Fig. 6e, Fig. S9e,f**). Additionally, also effector and NK-like T cell subsets strongly enriched for the 'better effector' signature, likely due to the high expression of effector genes characterizing these states. Thus, in human tumors the 'better effector' signature may either reflect a more general effector program that can be acquired by $CD8^+$ T cells or a cell state that emerges later upon IL2 treatment.

As a final experiment to understand whether the global transcriptional reprogramming upon CD8-IL2 was independent of immunological response, we performed a separate analysis of the one tumor (RE027) in our cohort that did not show an immunological response to CD8-IL2 (**Fig. 2a,3a**), reasoning that the T cells in this tumor should display IL2-induced changes that occur independent of concurrent TCR-signaling.

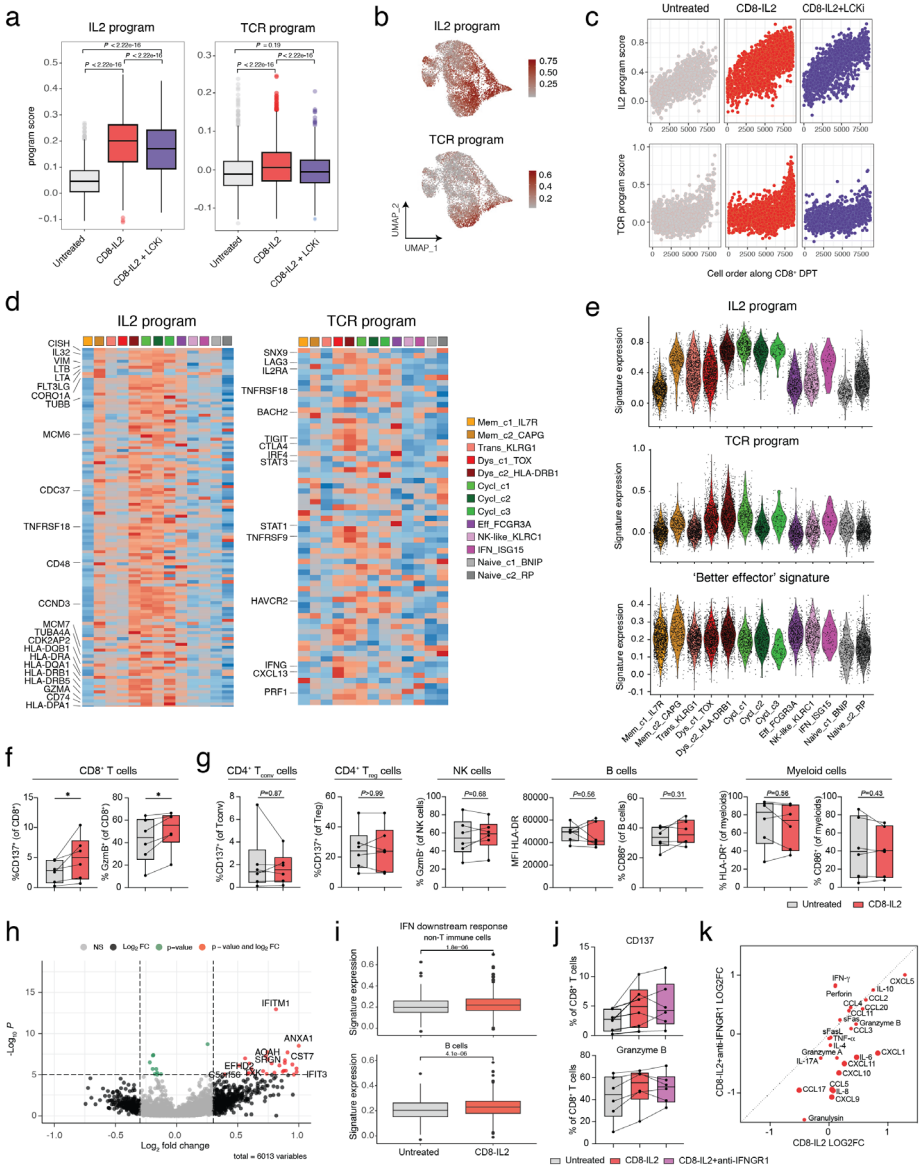

Figure 6. CD8⁺ T cells acquire distinct transcriptional programs following CD8-IL2 treatment dependent on antigen recognition. (a) IL2 program (123 genes) and TCR program (66 genes) scores in CD8⁺ T cells from the untreated, CD8-IL2 and CD8-IL2+LCKi conditions. **(b)** UMAP displaying the expression of the IL2 program and TCR program. **(c)** Expression of the IL2 program and TCR program for CD8⁺ T cells order along DPT in the untreated, CD8-IL2 and CD8-IL2+LCKi conditions. **(d)** Heatmaps displaying expression of the genes in the IL2 program and TCR program, respectively, in the different CD8⁺ T cell clusters. **(e)** Violin plots displaying IL2 program, TCR program, and 'better effector' signature expression in cells separated for the 13 different intratumoral CD8⁺ T cell clusters. **(f+g)** Quantification of activation and maturation markers in CD8⁺ T cells **(f)** and distinct immune populations **(g)** in untreated and CD8-IL2-treated PDTFs measured by flow cytometry (n=6). *$P < 0.05$ by two-tailed

Wilcoxon test. **(h)** Differential gene expression analysis of non-T immune cells between the untreated and CD8-IL2-treated condition in the 4 CD8-IL2-R tumors. **(i)** IFN downstream response signature in non-T immune (top) and B cells (bottom) from untreated and CD8-IL2-treated PDTFs. **(j)** Quantification of CD137 and Granzyme B expression on total $CD8^+$ T cells in PDTFs that were untreated or treated with CD8-IL2 and CD8-IL2+anti-IFNgR1, respectively (n=6). **(k)** Correlation of log2 fold changes (LOG2FC) of soluble mediators induced by either CD8-IL2 and CD8-IL2+anti-IFNgR1 versus the untreated condition. Parameters with fold change >2 between stimulated conditions are marked by a large dot. *P* values were calculated by two-tailed Wilcoxon test (a, f-i). *P* values were adjusted by Bonferroni correction (h).

Analysis of IL2 and TCR program dynamics revealed that the IL2 signature increased over pseudotime independently of TCR signaling in all tumors (**Fig. S10a**). In contrast, the TCR program was not detectable in RE027, both in untreated and treated conditions, suggesting absence of tumor recognition (**Fig. S10b**). Accordingly, comparison of individual clusters from each tumor revealed consistent IL2 program scores across induced clusters for all tumors, whereas TCR program scores were noticeably lower in the dysfunctional and Cycl_c1 and Cycl_c3 clusters in RE027 (**Fig. S10c**). Supporting the lack of a tumor-reactive repertoire in RE027, this tumor displayed substantially distinct clonal expansion patterns with most expanded TCRs found in the memory and effector, rather than dysfunctional cell compartments (**Fig. S10d**). Additionally, by directly comparing individual expanded T cell clones present in both the untreated and CD8-IL2-treated conditions, we observed that TCRs in tumors with immune reactivation upon CD8-IL2 transitioned into the Dys_c2_HLA-DRB1 or cycling clusters, whereas this transition could not be observed in the non-responding RE027 tumor (**Fig. S10e**). Collectively, these results support a mechanism in which CD8-IL2 profoundly rewires tumor-infiltrating T cells, endowing them with effector capacity, and thereby facilitates the reinvigoration of tumor-specific dysfunctional T cells to unleash potent antitumor immunity.

$CD8^+$ T cell-induced antitumor immunity is potentiated by TME-resident immune populations

To understand how CD8-IL2 treatment may alter the TME beyond the $CD8^+$ T cell pool, we performed PDTF cultures of six responsive tumors for 24 hrs. instead of 48 hrs., allowing better preservation of the innate immune compartment. After confirming that CD8-IL2 already activates $CD8^+$ T cells at this timepoint (**Fig. 6f**), we assessed the expression of activation and maturation markers on T_{conv}, T_{reg}, NK cell, B cell, and myeloid cell compartments (**Fig. 6g**). Aside from a small increase in CD86 expression on B cells in 4/6 tumors, no consistent phenotypic changes were observed across any of these subsets. To evaluate potential transcriptional changes, we performed differential gene expression analysis of all non-T immune cells between CD8-IL2-treated and untreated PDTFs. A limited number of genes was significantly upregulated upon CD8-IL2, including the IFN-inducible genes *IFITM1*, *IFIT3,* and *CCL5* (**Fig. 6h**). We thus hypothesized that the IFNγ produced by $CD8^+$ T cells upon reinvigoration may be sensed by other immune cells. To test this, we assessed the expression of IFN-responsive genes[60] which confirmed increased IFN-sensing upon CD8-IL2, both within the whole non-T immune cell compartment, and specifically within B cells which formed the largest subpopulation (**Fig. 6i**).

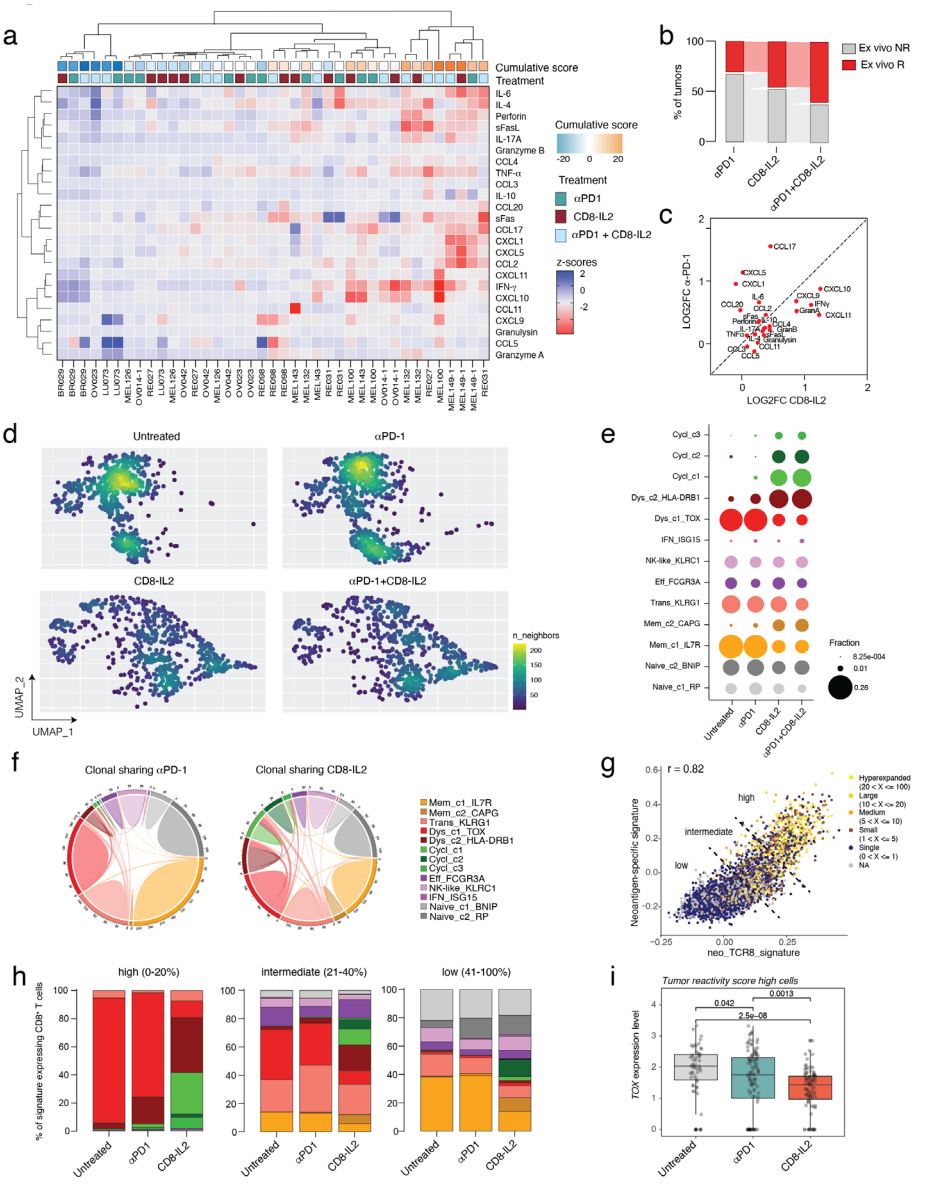

Figure 7. Reinvigoration of tumor-reactive T cells by CD8-IL2 is superior to PD-1 blockade. (a) Normalized delta values (CD8-IL2 condition, anti-PD-1 condition or anti-PD-1+CD8-IL2 condition – untreated condition) of soluble mediators secreted by PDTFs, ordered based on unsupervised hierarchical clustering. **(b)** Percentage of tumors displaying an ex vivo response (positive cumulative z-score) to anti-PD-1 (n=4/13), to CD8-IL2 (n=6/13) and to anti-PD-1+CD8-IL2 (n=8/13). **(c)** Correlation of log2 fold changes (LOG2FC) of concentrations of soluble mediators upon CD8-IL2 or anti-PD-1 treatment versus the untreated condition. **(d)** UMAP representation of $CD8^+$ T cell density from the untreated, CD8-IL2, anti-PD-1 and anti-PD-1+CD8-IL2 conditions for the three tumors responsive to ex vivo anti-PD-1. **(e)** $CD8^+$ T cell cluster distribution in PDTFs left untreated or treated with CD8-IL2, anti-PD-1, and anti-PD-1+CD8-IL2, respectively. **(f)** Circos plots displaying clonal sharing

of the different clusters in the untreated and anti-PD-1 conditions, and in the untreated and CD8-IL2 conditions, respectively. All clonotypes are included in the analysis. **(g)** Neoantigen-specific gene signature score[57] and Neo_TCR_8 score[59] for $CD8^+$ T cells from ex vivo anti-PD-1 responsive tumors color-coded by their clonal expansion. **(h)** Cluster distribution of tumor-reactive cells, defined in (g) as scoring top 20% (0-20%), intermediate (21-40%) or low (41-100%) for both tumor-reactive gene signatures in the untreated, anti-PD-1 and CD8-IL2 conditions. **(i)** *TOX* gene expression levels in cells scoring as top 20% for the tumor reactivity signatures in untreated, anti-PD-1 and CD8-IL2-treated PDTFs. *P* values calculated by two-tailed Wilcoxon test.

To directly test whether the alterations in the non-T cell immune compartment are dependent on IFNγ, we pretreated PDTFs with an anti-IFNγR antibody before CD8-IL2 treatment. While $CD8^+$ T cell activation remained unchanged by IFNγR-blockade, a number of soluble mediators were no longer produced when IFNγ signaling was inhibited, particularly affecting IFN-downstream chemokines such as CXCL9, CXCL10, and CXCL11 (**Fig. 6j,k**). Collectively, these data suggest that, through IFNγ, TME-resident immune cells may act as amplifiers of CD8-IL2-mediated T cell reinvigoration.

T cell reinvigoration by CD8-IL2 is qualitatively and quantitatively superior to PD-1 blockade

PD-1 signaling is a major inhibitory brake that prevents effector function of tumor-specific T cells. However, not all T cell-infiltrated tumors respond to PD-1 blockade. Therefore, we next compared CD8-IL2 and PD-1 blockade for their capacity to reactivate antitumor immunity. To this end, PDTFs from 13 tumors were treated with either CD8-IL2, anti-PD-1, or CD8-IL2+*anti*-PD-1. Hierarchical clustering of soluble mediators and cumulative score calculations discriminated samples with absence or presence of a downstream immune response (**Fig. 7a**). Of note, immunological responses were observed in all three treatment groups. We next evaluated the number of tumors exhibiting ex vivo responses to the different treatments (**Fig. 7b**). Among the 13 tumors, 4 (31%) responded to anti-PD-1, and interestingly, all these tumors also showed a response to CD8-IL2. Notably, two tumors that did not respond to anti-PD1 treatment displayed a response to CD8-IL2 (2/13; 15%). Upon combination treatment, additional two tumors that were resistant to either anti-PD-1 and CD8-IL2 monotherapy became immunologically responsive (2/13; 15%), indicating that overall CD8-IL2 converted 44% (4/9) of the anti-PD1 non-responders.

As all anti-PD-1 responders also responded to CD8-IL2, we next investigated whether the two treatments resulted in distinct or similar response patterns. To this end, we compared the changes in individual soluble mediators in ex vivo responders (cumulative score >0) to each treatment. While a large fraction of mediators were induced similarly by both treatments, some differences were noticeable (**Fig. 7c**). Specifically, the induction of IFNγ and its downstream mediators seemed more prominent upon CD8-IL2 than anti-PD-1 treatment, suggesting potential differences in T cell reactivation. Therefore, we next questioned how transcriptional reprogramming by *anti*-PD1 compared to that by CD8-IL2. Among the five tumors included for scRNA-seq, three were also ex vivo responders to PD-1 blockade, evidenced by a positive anti-PD-1 response score which was previously

found to be highly predictive for clinical response to PD-1 blockade[10] (**Fig. S5a+S11a**). Comparing the UMAP visualizations of the anti-PD-1 and CD8-IL2 conditions from the three dual responding tumors, we observed that the remodeling of cell states induced by anti-PD-1 was minor compared to that caused by CD8-IL2 (**Fig. 7d**), compatible with previous observations in mouse models[15,42]. By contrast, the anti-PD-1+CD8-IL2 combination led to similar effects as CD8-IL2 alone. Comparing the prevalence of individual clusters between treatments, we found that anti-PD-1 promoted a slight expansion of the Dys_c2_HLA-DRB1, and minimally of the Cycl_c1 clusters, which were substantially increased by CD8-IL2 alone or in combination with anti-PD-1 (**Fig. 7e**). As a control, we assessed the two anti-PD-1 non-responders, which did not show expansion of these clusters, suggesting a relation to the immunological responses observed (**Fig. S11b**).

Next, we aimed to assess whether the different treatments led to distinct transcriptional changes in the induced T cell clusters. As no apparent changes in cluster distribution were observed between the CD8-IL2 and CD8-IL2+anti-PD-1 conditions, we performed DGE analysis between the two treatments. This revealed only two genes (*GZMB* and *NSD2*) to be significantly different (**Fig. S11c**), suggesting that the prominent transcriptional effects of CD8-IL2 may make it difficult to capture additional anti-PD-1 effects. Similar observations have been made in mouse models, where the combination of PD-1 and IL2 led to equal effects as IL2 alone[15]. Consequently, we focused on comparing transcriptional changes elicited by the two monotherapies. To understand whether the treatments reinvigorate T cells originating from different cell states, we evaluated TCR sharing between cells in the untreated with those in either the anti-PD-1 or CD8-IL2 conditions (**Fig. 7f**). In this analysis, the anti-PD-1-induced Dys_c2_HLA_DRB1 and Cycl_c1 clusters displayed the largest clonal overlap with the Dys_c1_TOX cluster, and to some extent with the Trans_KLRG1 cluster, suggesting reinvigoration of these cell states. Of note, the three clusters that were formed by CD8-IL2 in the presence of TCR-signaling showed similar sharing patterns, with all exhibiting a strong overlap with the Dys_c1_TOX cluster. In addition, the Cycl_c1 cluster also displayed TCR sharing with the Trans_KLRG1 state, in line with the induction of proliferation of precursor-like T cells. Of note, the fraction of reinvigorated cells was substantially lower upon *anti*-PD-1 than upon CD8-IL2 (**Fig. 7d,f**). This was further corroborated when examining individual TCRs present in both the untreated and anti-PD-1 conditions, where only minor shifts in cell state were observed (**Fig. S11d**). Intriguingly, DPT analysis showed that dysfunctional T cells arising late in pseudotime displayed a clear increase in the TCR program upon anti-PD-1 treatment, suggesting that they may undergo reactivation despite largely maintaining their original dysfunctional state (**Fig. S11e**).

To characterize the differential effects of PD-1 blockade and CD8-IL2 in more detail, we focused on the tumor-reactive $CD8^+$ compartment. Therefore, we inferred tumor reactivity based on the expression of two published gene signatures[57,59]. Of note, expression of these signatures strongly correlated with clonal expansion and tumor recognition capacity observed in the sorted subsets (**Fig. 7g, Fig. S11f**). In untreated tumors, the highly-scored tumor-reactive cells (top 20%) were predominantly found in the dysfunctional cluster

Dys_c1_TOX (**Fig. 7h**). Conversely, the cells scoring either intermediate (21-40%) or low (41-100%) for these tumor reactivity signatures comprised a mix of various cell states with fewer or no dysfunctional T cells, respectively. Upon anti-PD-1 treatment, approximately one third of highly-scored tumor-reactive T cells acquired the activated Dys_c2_HLA-DRB1 state, with a minor fraction moving to the proliferative Cycl_c1 cluster. In contrast, upon CD8-IL2 the vast majority of these cells underwent activation, shifting to the Dys_c2_HLA-DRB1, Cycl_c1 and Cycl_c3 phenotypes. A similar but slightly less prominent effect of CD8-IL2 was observed on cells with intermediate tumor reactivity scores, whereas lowly-scored cells mainly acquired the TCR-independent Mem_c2-CAPG and Cycl_c2 states. In contrast, PD-1 blockade did not induce activation or proliferation of cells with intermediate and low tumor reactivity scores. CD8-IL2 in contrast to anti-PD-1 also strongly reduced *TOX* expression in dysfunctional, and particularly in cells with high tumor reactivity score (**Fig. 7i, Fig. S11g**), suggesting qualitative differences in reinvigoration. DGE analysis between highly-scored tumor-reactive cells in the untreated and either treated condition further demonstrated transcriptional activation, including an increase in genes related to HLA class II expression, cytotoxicity, and proliferation. Of note, the induction of proliferation was largely limited to CD8-IL2, which also transcriptionally activated a larger part of the tumor-reactive T cell pool as compared to anti-PD-1 (**Fig. S11h**). Altogether, our findings suggest that anti-PD-1 and CD8-IL2 may induce a similar trajectory of activation in tumor-reactive T cells present within in the human TME. However, CD8-IL2 may reinvigorate a broader tumor-specific T cell pool and generate more potent effector cells, establishing CD8-IL2 as a promising strategy to unleash antitumor immunity in human cancers.

Discussion

In this study, we performed a comprehensive analysis of T cell reinvigoration by a novel CD8-targeted IL2Rβγ agonist in human cancer tissue. Thereby, we observed that CD8-IL2 broadly reactivates the intratumoral T cell landscape, and specifically enables the revival of dysfunctional T cells to mediate immune reactivation upon antigen encounter. Reinvigoration by CD8-IL2 was superior to that by PD-1 blockade and could even mobilize antigen-specific T cells in anti-PD-1 resistant tumors.

IL2 therapy has been identified as a promising strategy to enhance T cell responses in ICB resistant tumors[17, 61-63]. However, the clinical value of systemic IL2 administration is limited by toxicity and immunosuppressive effects following T_{reg} activation[64-66]. We here demonstrate that targeting of IL2 to the CD8β-chain allows for selective and potent reactivation of $CD8^+$ T cells, requiring 1,000-fold lower concentrations than recombinant IL2 or an untargeted IL2Rβγ agonist, thus making it an attractive strategy for systemic cancer therapy. Similar cis-targeting approaches have recently been explored in a number of murine studies[15,16,42]. In these studies, IL2 was directed towards $PD\text{-}1^+$ T cells reasoning that PD-1 expression may mark the tumor-reactive T cell pool. Interestingly, when comparing CD8- and PD-1-targeting of IL2 we observed no substantial differences in $CD8^+$

T cell reactivation, which may be explained by the fact that the vast majority of $CD8^+$ T cells in human tumors expresses PD-1. Of note, PD-1 is also present on T_{regs}, and treatment with PD1-IL2 accordingly increased their proportion in contrast to CD8-IL2, highlighting CD8-targeting as a valid strategy to selectively enhance antitumor effector responses.

One intriguing observation we made relates to the 'duality' of the response induced by CD8-IL2. While CD8-IL2 could induce T cell activation in the majority of tumors across five cancer types, functional immune responses leading to the production of pro-inflammatory cytokines and chemokines were elicited in about 60% of tumors. Perturbation experiments revealed that these immunological responses depended on simultaneous antigen recognition by the T cells as IL2 could not restore functional activity when TCR signaling was inhibited. Importantly, these observations also highlight that expression of effector markers such as Granzyme B or IFNγ does not necessarily allow to infer functionality. A number of recent studies using engineered IL2 molecules to enhance anti-tumor or anti-viral immunity in mouse models reported the induction of 'better effector' cells similar to those generated in acute infections[15,16,42]. Interestingly, this 'better effector' state was different from the IL2-driven activation program that we identified early during reinvigoration and showed enrichment in both IL2-induced states and effector subsets already present in untreated tumors. Thus, the 'better effector' program may either reflect a more general effector program acquired by T cells in human cancers or show a substantial increase only later during treatment. Supporting the latter notion, *Moynihan et al.* observed in the accompanying article that a cluster compatible with 'better effectors' was not detectable after two days of CD8-IL2 treatment, but emerged on day 4. The IL2 activation program in contrast was acquired by multiple $CD8^+$ cell states early after CD8-IL2 treatment, suggesting a rapid and broad remodeling of the intratumoral T cell landscape towards enhanced effector capacity. The induction of this program was however not sufficient to promote immunological responses as tumors displaying cytokine production upon CD8-IL2 exhibited an additional activation trajectory prompted by antigen recognition and restricted to the dysfunctional axis. Increased clonal expansion and TCR sharing among the dysfunctional T cell clusters as well as their enriched capacity for tumor recognition further supported the role of the dysfunctional pool in mediating CD8-IL2-induced immune responses. While this is in sharp contrast to most studies in mouse models which observed the main effect of IL2 on stem-like T cells, a recent murine study investigating a PD-1-targeted low-affinity IL2 similarly reported preferential reinvigoration of $PD\text{-}1^+TIM3^+$ dysfunctional T cells[13]. A possible explanation for these differences may be the distinct timepoints of analysis for these studies. Whereas IL2-induced expansion of stem-like cells was observed after 10-14 days of treatment, the reinvigoration of dysfunctional T cells observed by us and Ren *et al.*[13] was captured after 2 and 3 days, respectively. These data can be reconciled by a model in which the early response to IL2 is mainly mediated by tumor-specific dysfunctional T cells already located at the tumor site, followed by an influx of stem-like 'resource' cells at later timepoints that sustain the response.

The observation that a large fraction of dysfunctional T cells can be reinvigorated is intriguing as they are often considered terminally exhausted and resistant to therapeutic reinvigoration. Of note, treatment of the same tumors with PD-1 blockade induced highly limited revival of dysfunctional T cells, in line with prior reports describing the accumulation of exhausted T cells upon anti-PD-1 likely due to an epigenetically fixed state that prevents major transcriptional rewiring[15,42,67,68]. These findings are also compatible with the recent observation in chronic LCMV models that *Stat5*, the major IL2R downstream signal, acts as an antagonist of *Tox*, a key transcription factor driving the epigenetic imprinting of exhaustion[69-72]. Notably, induction of *Stat5* activity using an orthogonal IL2:IL2Rβ pair led to increased functionality and reduced exhaustion, specifically decreasing *Tox* expression in $CD8^+$ T cells with established dysfunction[73]. This was accompanied by partial reprogramming of the epigenetic landscape, leading to increased accessibility of effector- (*Ifng*, *Gzma*, *Gzmb*, *Prf1*, *Fasl*) and proliferation-related (*Mki67*) peaks. Compatible with these observations, we observed that tumor-specific dysfunctional T cells strongly reduced *TOX* expression and acquired effector biology upon CD8-IL2. It will therefore be of interest to assess in future studies whether IL2-mediated signals can promote epigenetic reprogramming of dysfunctional T cells also in human cancers. Interestingly, despite the limited change in cell state, we observed that dysfunctional T cells acquired a TCR-driven activation program upon PD-1 blockade, which also related to immune reactivation of the same tumors, suggesting that these cells can regain some degree of functionality. CD8-IL2 activated dysfunctional T cells along a similar transcriptional trajectory as anti-PD-1, however with more and qualitatively superior effectors as evidenced by a higher IFNγ response in the PDTFs.

The broad efficacy of CD8-IL2 across cancer types, the observed immunological responses in ex vivo anti-PD-1 resistant tumors, and the potential synergistic effects of combining CD8-IL2 with anti-PD-1 posit this therapy as an attractive new treatment strategy for cancer patients. However, these results also raise new questions about the interplay between the two therapies and how CD8-IL2 exerts activity in anti-PD-1 resistant tumors. Conceivable explanations are that resistant tumors contain a tumor-reactive T cell pool that is either not susceptible to anti-PD-1 or for which PD-1 signaling is not the sole barrier preventing activation. However, further research is required to elucidate how PD-1 blockade and CD8-IL2 may synergize and be optimally combined for clinical application.

In conclusion, our study provides comprehensive insights into the therapeutic potential of CD8-IL2 and its ability to reinvigorate the intratumoral $CD8^+$ T cell landscape. Our findings are compatible with a model in which CD8-IL2 can broadly 'arm' T cells with effector capacity, enabling particularly the dysfunctional T cell pool to undergo functional reactivation upon target antigen encounter. Finally, this study also highlights precision targeting of immunomodulatory signals to specific immune cell populations as an attractive strategy to induce effective antitumor immunity.

Methods

Human tumor tissue processing

Human tumor tissue was collected from patients with cancer undergoing surgery for non-small cell lung cancer, ovarian cancer, melanoma, renal cell carcinoma and breast cancer at the Netherlands Cancer Institute/Antoni van Leeuwenhoek Hospital (NKI-AVL) between April 2017 and December 2022 (**Table S1**). The study was approved by NKI-AVL's institutional review board (CFMPB484) and performed in compliance with all ethical regulations. Patients of whom material was collected for the study consented in writing either by opt-out procedure or via prior written informed consent (after May 2018) to their tissue being available for research after diagnostic procedures have been completed.

Resected human tumor tissue was collected on ice in RPMI 1640 (Thermo Fisher Scientific) supplemented with 2.5% fetal bovine serum (FBS) (Sigma-Aldrich) and 1% penicillin-streptomycin (Roche). Directly after collection, tumor tissues were dissected into fragments (PDTFs) of 1 to 2 mm^3 on ice. Processed tumor fragments were mixed to obtain collections of 8 to 12 fragments that represent different areas of the tumor. Each collection of fragments was frozen in 1 mL freezing medium (FBS with 10% dimethyl sulfoxide (Sigma-Aldrich)). Vials were cryopreserved in liquid nitrogen until further use.

Patient-derived tumor fragment cultures

PDTF cultures were performed as described previously[10,32]. In brief, cryopreserved PDTFs were thawed and washed with wash medium [Dulbecco's modified Eagle's medium (DMEM) supplemented with 10% FCS and 1% penicillin-streptomycin]. Subsequently, PDTFs were embedded in artificial extracellular matrix {sodium bicarbonate (1.1%; Sigma-Aldrich), rat-tail collagen I (1 mg/ml; Corning), Matrigel (2 mg/mL; Matrix High Concentration, Phenol Red-Free, BD Biosciences or Cultrex UltiMatrix, reduced growth factor basement membrane extract, R&D systems), tumor medium [DMEM supplemented with 1 mM sodium pyruvate (Sigma-Aldrich), 1× MEM non-essential AA (Sigma-Aldrich), 2 mM l-glutamine (Thermo Fisher Scientific), 10% FBS, and 1% penicillin-streptomycin]} as follows; 40 µL extracellular matrix was added to a flat-bottom 96-well plate and incubated at 37°C for 15-30 min. PDTFs were placed on top, and additional 40 µl of matrix were added and incubated at 37°C for 15-30 min. To treat the PDTFs ex vivo, tumor medium was supplemented with either CD8-IL2 (CD8-specific cis-targeting not-alpha attenuated-beta IL2, Asher Biotherapeutics, 10 nM for comparison to PD1-IL2, 1 nM for all other experiments,), PD1-IL2 (PD-1-specific cis-targeting not-alpha attenuated-beta IL2, Asher Biotherapeutics, 10 nM), IL2v (not-alpha IL2, Asher Biotherapeutics, 1 nM), anti-CD8β (clone 97/47, Asher Biotherapeutics, 1nM), recombinant human IL2 (Peprotech, see titration), recombinant human IL-15 (Preprotech, 1mM), anti-PD-1 (Nivolumab, Bristol-Myers Squibb, 10 µg/mL), or anti-CD3 (OKT3, BioLegend, 0.5 µg/mL). PDTF cultures were incubated for 48 hrs. at 37 °C. A shorter culture time of 24 hrs. was used for a subset of experiments as indicated. For response perturbations, PDTFs were preincubated for 2 hrs. at 37°C with either an Lcki (8 µM,

CAS no. 213743-31-8, Merck Millipore), anti-IFNGR1 (50µg/mL, catalog no. 92101, R&D systems), or anti-MHC I (100µg/mL, clone W6/32, Biolegend). To exclude toxicity induced by the LCKi, different gene signatures associated with cell death and stress were assessed[73], which did not show any increase in LCKi-treated compared to untreated PDTFs (**Fig. S12**).

PDTF culture processing and flow cytometry

After 48 hrs. of ex vivo tumor culture, supernatants were collected and frozen at -80°C, and PDTFs were pooled per condition in 2 mL ice-cold digestion medium [RPMI 1640 with 1% penicillin-streptomycin, Pulmozyme (12.6 µg/ml, Roche), and collagenase type IV (1 mg/mL, Sigma-Aldrich)]. PDTFs were digested at 37°C under continuous rotation for 45 to 60 min, washed with phosphate-buffered saline (PBS), filtered and subsequently transferred to a 96-well plate for the flow cytometry staining procedure. First, the cells were incubated with human Fc-Receptor Blocking Reagent (eBioscience) and simultaneously stained with Live/Dead IR Dye (Thermo Fisher Scientific) or Zombie NIR (BioLegend) for 20 min on ice. Next, cells were washed, incubated with the surface antibody mix in staining buffer (eBioscience) for 20 min on ice. After washing, cells were fixed and permeabiized using Fix/Perm solution (eBioscience) for 30 min at RT. Cells were subsequently washed twice with 1x permeabilization buffer (eBioscience) and incubated with the intracellular antibody mix in permeabilization buffer for 40 min at RT. Next, cells were washed twice and resuspended in FACS buffer [PBS supplemented with 2 mM Ethylenediaminetetraacetic acid (EDTA)] for data acquisition on a Symphony A5 (BD Bioscience) or Aurora (Cytek Bio). All antibodies used are listed in **Table S2**. Data analysis was performed with FlowJo software (version 10.7).

Analysis of soluble mediators

Supernatants collected from PDTF cultures were thawed on ice and pooled for each experimental condition (8-10 blocks per condition). The presence of indicated cytokines, chemokines and cytotoxic mediators was detected using the LEGENDplex Human CD8/NK panel and Human Proinflammatory Chemokine panels (both BioLegend). For all assays, 17 µl of volume were used, otherwise the assays were performed according to the manufacturer's instructions and measured on a BD LSR Fortessa™ X-20 Cell Analyzer (BD Bioscience).

Degranulation and IFNγ assay

To assess degranulation of intratumoral T cells upon CD8-IL2, cryopreserved PDTFs were thawed and digested as described above. Tumor digests were plated in a round-bottom 96-well plate and rested for 1 hr. Cells were subsequently stimulated with CD8-IL2 (1 nM) in the presence of anti-CD107a-FITC (1:50, Biolegend). After 1 hr., GolgiPlug (1:1000) and GolgiStop (1:1500) (both from BD Biosciences) were added, and the digest cultures were incubated for 6 hrs. to assess degranulation and overnight for IFNγ production. Afterwards, the samples were subjected to the flow cytometry staining procedure as described above and measured on an Aurora (Cytek Bio) analyzer.

Sorting and in vitro expansion of tumor-infiltrating lymphocytes (TILs)

To isolate different populations of $CD8^+$ TILs, cryopreserved PDTFs were thawed and digested as described above. Cells were washed with Cell Staining Buffer (Biolegend), resuspended in 300 µL PBS with Human TruStain FcX (1:10, Biolegend) and incubated for 10 min on ice. Next, cells were washed and incubated with 300 µL staining buffer containing anti-CD8-FITC (1:50, Biolegend), anti-CD127-PE-Cy7 (1:100, Biolegend), anti-CD39-BV711 (1:50, BD Biosciences), anti-CD62L-PE (1:50, Biolegend), anti-KLRG1-BV421 (1:20, Biolegend) and anti-PD1-AF647 (1:20, BD Biosciences) for 20 min on ice. DAPI was added shortly before the sort, and cells were subsequently sorted on the BD FACSAria Fusion SORP cell sorter (v.8.0.1; BD Bioscience) into four populations: 1) dysfunctional T cells ($CD8^+$ $CD39^+$ $PD1^+$), memory-like T cells ($CD8^+$ $CD127^+$), transitional T cells ($CD8^+$ $PD1^{int}$ $KLRG1^+$), and effector-like T cells ($KLRG1^+$). Sorted cells were collected in 1 mL cold TIL medium [80% RPMI/20% AIM-V (Thermo Fisher Scientific), 1% penicillin-streptomycin, 1% L-glutamine, 10% human serum (Sigma- Aldrich)]. Cells were rested for 3 hrs. in TIL medium supplemented with 30 IU/mL in IL2 (Clinigen Healthcare Ltd). Subsequently, TILs were expanded in vitro in the presence of 1:200 feeder cells (PBMCs irradiated at 40 Gy) and TIL medium supplemented with 30 ng/mL anti-CD3 (OKT3, Biolegend) and 3,000 IU/mL IL2 at 37°C. From day 7 onward, the cells were split 1:2 when necessary and medium supplemented with 3,000 IU/mL IL2 was refreshed. On day 14, cells were frozen and stored in liquid nitrogen.

Tumor reactivity co-culture

One day prior to co-culture, cryopreserved TILs were thawed and rested in TIL medium with low dose IL2 (30 IU/mL) overnight. Matched PDTFs were thawed, digested and rested in co-culture media [RPMI supplemented with 1% sodium pyruvate, 1% MEM non-essential AA, 0.2% penicillin/streptomycin, 10% human serum] for 1 hr at 37°C. Expanded TILs were stained with CellTrace Violet (CTV) according to the manufacturer's protocol (Thermo Fisher Scientific). The percentage of tumor cells from total live cells in digests were assessed by previous flow cytometry gating on $CD45^-$, forward and side scatter-high cells. 50-100k of CTV-labelled TILs were cocultured with autologous tumor digest at an effector:tumor ratio of 1:1 in co-culture medium, in the presence or absence of CD8-IL2 (10 nM). As a positive control, TILs were stimulated with anti-CD3 (OKT3, Biolegend, 10 µg/mL) and anti-CD28 (CD28.2, Biolegend, 5 µg /mL). To detect degranulation, anti-CD107a-FITC (1:50, Biolegend) was added to the co-culture. For analysis of IFNg, TNFa and CD107a expression, GolgiPlug (1:1000) and GolgiStop (1:1500) (both from BD Biosciences) were added after 1 hr., and the co-cultures were incubated for 12 to 16 hrs at 37°C. Afterwards, the samples were subjected to the flow cytometry staining procedure as described above and measured on an Aurora (Cytek Bio) analyzer.

Sample processing for single-cell RNA- and TCR-sequencing

For scRNAseq, PDTF cultures were processed as described above until a single cell suspension was obtained. Subsequently, cells were transferred to 1.5 mL Eppendorf tubes and resuspended in 25 µL cold Cell Staining Buffer (Biolegend) with Human TruStain FcX

(1:10, Biolegend) and incubated for 10 min on ice. In order to pool samples for sequencing, TotalSeq-C anti-human hashtag antibodies (numbers 1, 2, 4, 6, 7, 8, 9 and 10, 1 µg/ml final concentration, Biolegend) were added to the individual samples. Without washing, 25 µL of Cell Staining buffer containing anti-CD45-PerCP-Cy5.5 (1:50, Invitrogen) was added, accompanied by TotalSeq-C antibodies against PD-1 (EH12.1, 1:1000), CD8 (SK1, 1:5000) and CD4 (RPA-T4, 1:2500). Subsequently, cells were incubated for 25 min on ice and washed three times with 1 mL staining buffer. Then, cells were resuspended in 500 µL MACS buffer [PBS with 0.5% bovine serum albumin (BSA, Sigma) and 2 mM Ethylenediaminetetraacetic acid (EDTA, Life Technologies)]. To pool equal cell numbers of each sample labeled with the different hashtag antibodies, aliquots of 5 µL from each sample were counted using AccuCount Blank Particles 13.0-17.9 µm (Spherotech). Dead cells were stained with propidium iodide (PI, Sigma Aldrich, 0.5 µg/ml) right before acquisition. Using flow cytometry, live immune cells were counted per 10,000 counting beads to pool equal numbers of each sample. $CD45^+$ live cells from this mixture were subsequently sorted using a FACSAria Fusion Flow Cytometer (BD Biosciences) and collected in RPMI 1640 medium supplemented with 1% penicillin-streptomycin and 10% human serum. Lastly, cells were washed once with cold 1% BSA in PBS and once with 0.04% BSA in PBS, and resuspended in 0.04% BSA at a concentration between 800 and 1200 cells/µL for 10X Genomics scRNA&TCRseq.

Single-cell RNA-sequencing and TCR-sequencing

For scRNA&TCRseq, sorted $CD45^+$ immune cells were loaded on each lane of the 10X Chromium instrument at target capture rate of 1,000 to 10,000 individual cells per sample. Libraries of RNA, TCRs and antibody barcodes were constructed according to the manufacturer's protocol using the Chromium Next GEM Single Cell V(D)J Reagent Kits (10X Genomics). These libraries were sequenced on a Novaseq instrument (Illumina) with read lengths of 26-28/58-130 for RNA and HTO libraries, and 26-28/92-130 for TCR libraries, aimed at recovery of 30,000 read pairs per cell for RNA libraries, and 5,000 reads for both antibody and TCR libraries.

Single-cell data processing

Sequenced gene expression reads were mapped to the human GRCh38-2020-A reference genome and quantified using Cell Ranger software (10X Genomics, v7.1.0). The resulting filtered gene expression matrix and CITE-seq antibody count matrix were imported into Seurat (v4.9.9). Seurat objects were constructed on a per-patient basis and included all conditions, which were individually labeled using barcoded hashtag oligos (HTOs). Cells without dominant HTO signal or more than 1 dominant HTO were removed. The resulting datasets were merged. To ensure high data quality, cells were considered low quality and removed when they showed a mitochondrial RNA content of >15%, a ribosomal protein content < 7.5%, a unique molecular identifier (UMI) count <800, or displayed a UMI count lower than 500 or exceeding 6,000.

TCR data processing

Cell Ranger software (10x Genomics, v7.1.0) was used to assemble TCR reads into consensus sequences. Cells for which multiple TCRβ chains were captured were considered doublets and were removed from downstream analysis. Cells with a matching TCRα and TCRβ sequence were considered T cell clones.

Immune cell clustering

The transcripts counts of cells that passed quality control were log10-normalized using Seurat's NormalizeData() to correct for differences in library size. CITE-seq counts were normalized using center-log ratio (CLR), likewise using NormalizeData(). Highly variably expressed genes were selected using FindVariableFeatures(), with the selection.method set to "vst" and number of genes set to 2,000. From the list of 2,000 genes, we excluded genes that contained the sequence "MT-", "RP-", "LINC-", "AC-" in their name, as well as long-non coding RNAs "MALAT1" and "XIST". IG genes ("IG[HJKL]") and TCR V genes ("TRAV-" and TRBV-") were likewise excluded to avoid formation of clusters based on clonal populations. The genes that remained after filtering were used for principal component analysis using runPCA() after gene expression was scaled and the effects of mitochondrial genes and dissociation induced genes were regressed out using ScaleData(). The first 20 principal components were selected as input for UMAP (RunUMAP()) and clustering. Clusters of transcriptionally similar cells were identified by constructing a k-nearest neighbors graph and applying the Louvain algorithm with resolution set at 1.5, using the FindNeighbors() and Findclusters() functions respectively.

Filtering CD8⁺ T cells

The resulting clusters were annotated as either "B cell", "CD4 T cell", "CD8 T cell", "gd T cell & NK cell". We noticed that the CD4/CD8 T cell annotation was imperfect and observed signal of $CD4^+$ T cells within the CD8 clusters and vice versa. To maximize correct separation of $CD4^+$ T cells and $CD8^+$ T cells and minimize false positive events for either compartment, we applied a series of filters. First, among the cells previously annotated as "CD4 T cell", "CD8 T cell" and "γδ T cell & NK cell", we selected all cells that showed a normalized expression > 0.5 of either *CD3D*, *CD3E* or *CD3G*. Among these $CD3^+$ cells, cells with normalized expression of CD4 CITE-seq antibody > 0.7 or expression of *CD4* > 0.5 were annotated as "$CD4^+$ T cell". Likewise, cells that showed normalized expression of the CD8 CITE-seq antibody > 1.2 or expression of *CD8A* > 0.5 or *CD8B* > 0.5 were annotated as $CD8^+$ T cell. Cells that passed both the CD4 and CD8 filtering steps were annotated as "Double positive" and were not included in further downstream analysis.

Cell state analysis

The resulting cells that classified as "$CD8^+$ T cells" were reclustered in order to derive more detailed $CD8^+$ T cell subsets. The 4,000 most variable features were identified as outlined previously. IG genes and TCR genes were again excluded from this list. Data were scaled and the effects of mitochondrial genes were regressed out. To remove any batch effects that

might arise, CD8+ T cells from the five patients were integrated using the RunHarmony() function from Seurat, with the max.iter.harmony parameter set to 30. UMAP projections were created using the first 16 dimensions (reduction set to 'harmony') and clusters were derived similar as described earlier (resolution Louvain algorithm set to 0.8).

CD8+ T cell subset annotation

Seurat's FindAllMarkers() function was used to obtain genes that were differentially expressed between clusters and to identify canonical markers that defined each cluster. Furthermore, to better identify various CD8+ T cell subtypes, we applied gene signatures for terminally exhausted CD8+ T cells[51], effector T cells[50], memory T cells[51] and proliferating T cells[53]. Scores for each signature were computed using the Seurat function AddModuleScore() using the gene signature of interest and setting the number of control genes from the same bin of expression at 5. The same strategy was used to compute the better effector signature from Codarri Deak *et al.*,[42] in this dataset, using the genes with FDR < 0,01.

Development of IL2 and TCR gene programs

To identify a TCR-specific gene signature, independent of CD8-IL2 exposure, we derived genes that were upregulated in T cells upon treatment with anti-CD3 compared to T cells that were untreated. For this, we compared gene expression of all CD8+ T cells in the untreated condition to all CD8+ T cells in the anti-CD3-treated condition using Seurat's FindMarkers() function. All genes that were enriched with an average log2 fold change > 0.3 and p value < 0.05 in the anti-CD3 condition were included in the signature. A similar approach was used to compile a signature of genes induced upon CD8-IL2 treatment independent of TCR signaling. To this end, transcriptomic differences between cells that were untreated or treated with CD8-IL2+LCKi were identified. The TCR program score and IL2 program score were calculated for each cell using AddModuleScore().

Pseudotime analysis and trajectory inference

To model transitions between CD8+ T cell subsets, DPT analysis was performed to construct differentiation trajectories. The first 20 harmony-corrected principal components were used as input to derive a diffusion map with 30 principal components, using the DiffusionMap() function (default parameters) from Destiny (V3.14). DPT was calculated by inputting the diffusion map into the DPT() function to rank the cells.

TCR analysis

TCR annotation was performed using the 10X cellranger vdj pipeline. If more than one b chain was detected in a cell, then the cell was considered as doublet and excluded from further analysis. scRepertoire package (v.1.10.0) was used for clonotype assignment and analysis of clonotype dynamics. To compare differences in CD8+ T cell state between cells from different conditions, we performed clone-matched analysis of the cell state composition of clones derived from untreated and CD8-IL2 conditions, or untreated and

anti-PD-1-treated conditions. Only clones that were present at least once in each condition were included.

Statistical analysis

Data are reported as the mean ± s.e.m.. Statistical significance was determined using the Mann–Whitney *U*-test, two-tailed Wilcoxon test or Friedman test, as indicated. Differences were considered statistically significant if ****$P < 0.0001$, ***$P < 0.001$, **$P < 0.01$, **$P < 0.05$. All analyses were performed in either Graphpad (v.9.5.1) or R (v.4.2.3). Unless otherwise specified, experiments were performed without duplicates because of material restrictions.

Data and code availability

Source data are provided with this paper. The scRNA&TCRseq data generated in this study are deposited in the European Genome-Phenome Archive (EGA) under accession number EGAS00001007712 and are accessible upon request. For inquiries regarding data access or any related information, please contact bibliotheek@nki.nl. Other data supporting this report are available from the corresponding author upon reasonable request.

References

1. June CH. Adoptive T cell therapy for cancer in the clinic. J Clin Invest. American Society for Clinical Investigation; 2007;117:1466–76.
2. June CH, O'Connor RS, Kawalekar OU, Ghassemi S, Milone MC. CAR T cell immunotherapy for human cancer. Science. American Association for the Advancement of Science; 2018;359:1361–5.
3. Schumacher TN, Schreiber RD. Neoantigens in cancer immunotherapy. Science. 2015;348:69–74.
4. Rosenberg SA, Restifo NP. Adoptive cell transfer as personalized immunotherapy for human cancer. Science. 2015;348:62–8.
5. Sharma P, Goswami S, Raychaudhuri D, Siddiqui BA, Singh P, Nagarajan A, et al. Immune checkpoint therapy—current perspectives and future directions. Cell. 2023;186:1652–69.
6. Yost KE, Satpathy AT, Wells DK, Qi Y, Wang C, Kageyama R, et al. Clonal replacement of tumor-specific T cells following PD-1 blockade. Nat Med. Nature Publishing Group; 2019;25:1251–9.
7. Wu TD, Madireddi S, de Almeida PE, Banchereau R, Chen Y-JJ, Chitre AS, et al. Peripheral T cell expansion predicts tumour infiltration and clinical response. Nature. 2020;579:274–8.
8. Schietinger A, Philip M, Krisnawan VE, Chiu EY, Delrow JJ, Basom RS, et al. Tumor-Specific T Cell Dysfunction Is a Dynamic Antigen-Driven Differentiation Program Initiated Early during Tumorigenesis. Immunity. 2016;45:389–401.
9. Zhang J, Ji Z, Caushi JX, El Asmar M, Anagnostou V, Cottrell TR, et al. Compartmental Analysis of T-cell Clonal Dynamics as a Function of Pathologic Response to Neoadjuvant PD-1 Blockade in Resectable Non-Small Cell Lung Cancer. Clin Cancer Res Off J Am Assoc Cancer Res. 2020;26:1327–37.
10. Voabil P, de Bruijn M, Roelofsen LM, Hendriks SH, Brokamp S, van den Braber M, et al. An ex vivo tumor fragment platform to dissect response to PD-1 blockade in cancer. Nat Med. Nature Research; 2021;27:1250–61.
11. Tumeh PC, Harview CL, Yearley JH, Shintaku IP, Taylor EJM, Robert L, et al. PD-1 blockade induces responses by inhibiting adaptive immune resistance. Nature. Nature Publishing Group; 2014;515:568–71.
12. Schomburg A, Menzel T, Körfer A, Heer G, Dallmann I, Kirchner H, et al. In vivo and ex vivo antitumor activity in patients receiving low-dose subcutaneous recombinant interleukin-2. Nat Immun. 1992;11:133–43.
13. Ren Z, Zhang A, Sun Z, Liang Y, Ye J, Qiao J, et al. Selective delivery of low-affinity IL-2 to PD-1+ T cells rejuvenates antitumor immunity with reduced toxicity. J Clin Invest. 2022;132:e153604.
14. Wu W, Chia T, Lu J, Li X, Guan J, Li Y, et al. IL-2Rα-biased agonist enhances antitumor immunity by invigorating tumor-infiltrating CD25+CD8+ T cells. Nat Cancer. 2023;4;1309-1325
15. Hashimoto M, Araki K, Cardenas MA, Li P, Jadhav RR, Kissick HT, et al. PD-1 combination therapy with IL-2 modifies CD8+ T cell exhaustion program. Nature. Nature Publishing Group; 2022;610:173–81.
16. Tichet M, Wullschleger S, Chryplewicz A, Fournier N, Marcone R, Kauzlaric A, et al. Bispecific PD1-IL2v and anti-PD-L1 break tumor immunity resistance by enhancing stem-like tumor-reactive CD8+ T cells and reprogramming macrophages. Immunity. 2023;56:162-179.e6.
17. Kaptein P, Jacoberger-Foissac C, Dimitriadis P, Voabil P, de Bruijn M, Brokamp S, et al. Addition of interleukin-2 overcomes resistance to neoadjuvant CTLA4 and PD1 blockade in ex vivo patient tumors. Sci Transl Med. 2022;14:eabj9779.
18. Rosenberg SA. IL-2: the first effective immunotherapy for human cancer. J Immunol Baltim Md 1950. 2014;192:5451–8.
19. O'Gorman WE, Dooms H, Thorne SH, Kuswanto WF, Simonds EF, Krutzik PO, et al. The initial phase of an immune response functions to activate regulatory T cells. J Immunol Baltim Md 1950. 2009;183:332–9.

20. Kalia V, Sarkar S, Subramaniam S, Haining WN, Smith KA, Ahmed R. Prolonged interleukin-2Ralpha expression on virus-specific CD8+ T cells favors terminal-effector differentiation in vivo. Immunity. 2010;32:91–103.
21. Rosenzwajg M, Lorenzon R, Cacoub P, Pham HP, Pitoiset F, El Soufi K, et al. Immunological and clinical effects of low-dose interleukin-2 across 11 autoimmune diseases in a single, open clinical trial. Ann Rheum Dis. 2019;78:209–17.
22. Hartemann A, Bensimon G, Payan CA, Jacqueminet S, Bourron O, Nicolas N, et al. Low-dose interleukin 2 in patients with type 1 diabetes: a phase 1/2 randomised, double-blind, placebo-controlled trial. Lancet Diabetes Endocrinol. 2013;1:295–305.
23. Rosenberg SA, Yang JC, Topalian SL, Schwartzentruber DJ, Weber JS, Parkinson DR, et al. Treatment of 283 consecutive patients with metastatic melanoma or renal cell cancer using high-dose bolus interleukin 2. JAMA. 1994;271:907–13.
24. Krieg C, Létourneau S, Pantaleo G, Boyman O. Improved IL-2 immunotherapy by selective stimulation of IL-2 receptors on lymphocytes and endothelial cells. Proc Natl Acad Sci U S A. 2010;107:11906–11.
25. Kim DW, Zloza A, Broucek J, Schenkel JM, Ruby C, Samaha G, et al. Interleukin-2 alters distribution of CD144 (VE-cadherin) in endothelial cells. J Transl Med. 2014;12:113.
26. Sun Z, Ren Z, Yang K, Liu Z, Cao S, Deng S, et al. A next-generation tumor-targeting IL-2 preferentially promotes tumor-infiltrating CD8+ T-cell response and effective tumor control. Nat Commun. 2019;10:3874.
27. Ghelani A, Bates D, Conner K, Wu M-Z, Lu J, Hu Y-L, et al. Defining the Threshold IL-2 Signal Required for Induction of Selective Treg Cell Responses Using Engineered IL-2 Muteins. Front Immunol. 2020;11:1106.
28. Sim GC, Liu C, Wang E, Liu H, Creasy C, Dai Z, et al. IL2 Variant Circumvents ICOS+ Regulatory T-cell Expansion and Promotes NK Cell Activation. Cancer Immunol Res. 2016;4:983–94.
29. Charych DH, Hoch U, Langowski JL, Lee SR, Addepalli MK, Kirk PB, et al. NKTR-214, an Engineered Cytokine with Biased IL2 Receptor Binding, Increased Tumor Exposure, and Marked Efficacy in Mouse Tumor Models. Clin Cancer Res Off J Am Assoc Cancer Res. 2016;22:680–90.
30. Sharma M, Khong H, Fa'ak F, Bentebibel S-E, Janssen LME, Chesson BC, et al. Bempegaldesleukin selectively depletes intratumoral Tregs and potentiates T cell-mediated cancer therapy. Nat Commun. 2020;11:661.
31. Diab A, Tykodi SS, Daniels GA, Maio M, Curti BD, Lewis KD, et al. Bempegaldesleukin Plus Nivolumab in First-Line Metastatic Melanoma. J Clin Oncol. Wolters Kluwer; 2021;39:2914–25.
32. Moynihan KD, Kumar MP, Sultan H, Pappas DC, Park T, Chin SM, et al. IL2 Targeted to CD8+ T cells promotes robust effector T-cell responses and Potent Antitumor immunity. *Cancer Discovery*. 2024;14:1206-25
33. Roelofsen LM, Voabil P, de Bruijn M, Herzig P, Zippelius A, Schumacher TN, et al. Protocol for ex vivo culture of patient-derived tumor fragments. STAR Protoc. 2023;4:102282.
34. Dudley ME, Wunderlich JR, Robbins PF, Yang JC, Hwu P, Schwartzentruber DJ, et al. Cancer regression and autoimmunity in patients after clonal repopulation with antitumor lymphocytes. Science. 2002;298:850–4.
35. Boon T, Coulie PG, Van den Eynde BJ, van der Bruggen P. Human T cell responses against melanoma. Annu Rev Immunol. 2006;24:175–208.
36. Ring AM, Lin J-X, Feng D, Mitra S, Rickert M, Bowman GR, et al. Mechanistic and structural insight into the functional dichotomy between IL-2 and IL-15. Nat Immunol. 2012;13:1187–95.
37. Peace DJ, Cheever MA. Toxicity and therapeutic efficacy of high-dose interleukin 2. In vivo infusion of antibody to NK-1.1 attenuates toxicity without compromising efficacy against murine leukemia. J Exp Med. 1989;169:161–73.
38. Assier E, Jullien V, Lefort J, Moreau J-L, Di Santo JP, Vargaftig BB, et al. NK cells and polymorphonuclear neutrophils are both critical for IL-2-induced pulmonary vascular leak syndrome. J Immunol Baltim Md 1950. 2004;172:7661–8.

39. Zheng L, Qin S, Si W, Wang A, Xing B, Gao R, et al. Pan-cancer single-cell landscape of tumor-infiltrating T cells. Science. 2021;374:abe6474.
40. van der Leun AM, Schumacher TN. An atlas of intratumoral T cells. Science. 2021;374:1446–7.
41. Gueguen P, Metoikidou C, Dupic T, Lawand M, Goudot C, Baulande S, et al. Contribution of resident and circulating precursors to tumor-infiltrating CD8+ T cell populations in lung cancer. Sci Immunol. 2021;6:eabd5778.
42. Codarri Deak L, Nicolini V, Hashimoto M, Karagianni M, Schwalie PC, Lauener L, et al. PD-1-cis IL-2IR agonism yields better effectors from stem-like CD8+ T cells. Nature. Nature Publishing Group; 2022;610:161–72.
43. Duhen T, Duhen R, Montler R, Moses J, Moudgil T, de Miranda NF, et al. Co-expression of CD39 and CD103 identifies tumor-reactive CD8 T cells in human solid tumors. Nat Commun. Nature Publishing Group; 2018;9:2724–2724.
44. Simoni Y, Becht E, Fehlings M, Loh CY, Koo SL, Teng KWW, et al. Bystander CD8+T cells are abundant and phenotypically distinct in human tumour infiltrates. Nature. Springer US; 2018;557:575–9.
45. Borsellino G, Kleinewietfeld M, Di Mitri D, Sternjak A, Diamantini A, Giometto R, et al. Expression of ectonucleotidase CD39 by Foxp3+ Treg cells: hydrolysis of extracellular ATP and immune suppression. Blood. 2007;110:1225–32.
46. Ahlmanner F, Sundström P, Akeus P, Eklöf J, Börjesson L, Gustavsson B, et al. CD39+ regulatory T cells accumulate in colon adenocarcinomas and display markers of increased suppressive function. Oncotarget. 2018;9:36993–7007.
47. Thommen DS, Koelzer VH, Herzig P, Roller A, Trefny M, Dimeloe S, et al. A transcriptionally and functionally distinct pd-1+ cd8+ t cell pool with predictive potential in non-small-cell lung cancer treated with pd-1 blockade. Nat Med. Nature Publishing Group; 2018;24:994–1004.
48. Kaptein P, Thommen DS. Keeping track of the T cells that matter. Nat Cancer. NLM (Medline); 2022;3:1015–7.
49. Liu B, Zhang Y, Wang D, Hu X, Zhang Z. Single-cell meta-analyses reveal responses of tumor-reactive CXCL13+ T cells to immune-checkpoint blockade. Nat Cancer. Nature Publishing Group; 2022;3:1123–36.
50. Sanchez-Paulete AR, Labiano S, Rodriguez-Ruiz ME, Azpilikueta A, Etxeberria I, Bolaños E, et al. Deciphering CD137 (4-1BB) signaling in T-cell costimulation for translation into successful cancer immunotherapy. Eur J Immunol. 2016;46:513–22.
51. Pace L, Goudot C, Zueva E, Gueguen P, Burgdorf N, Waterfall JJ, et al. The epigenetic control of stemness in CD8+ T cell fate commitment. Science. 2018;359:177–86.
52. Guo X, Zhang Y, Zheng L, Zheng C, Song J, Zhang Q, et al. Global characterization of T cells in non-small-cell lung cancer by single-cell sequencing. Nat Med. 2018;24:978–85.
53. Tirosh I, Izar B, Prakadan SM, Wadsworth MH, Treacy D, Trombetta JJ, et al. Dissecting the multicellular ecosystem of metastatic melanoma by single-cell RNA-seq. Science. American Association for the Advancement of Science; 2016;352:189–96.
54. van der Leun AM, Thommen DS, Schumacher TN. CD8+ T cell states in human cancer: insights from single-cell analysis. Nat Rev Cancer. Nature Research; 2020;20:218–32.
55. Wherry EJ, Ha S-J, Kaech SM, Haining WN, Sarkar S, Kalia V, et al. Molecular Signature of CD8+ T Cell Exhaustion during Chronic Viral Infection. Immunity. 2007;27:670–84.
56. Haghverdi L, Büttner M, Wolf FA, Buettner F, Theis FJ. Diffusion pseudotime robustly reconstructs lineage branching. Nat Methods. Nature Publishing Group; 2016;13:845–8.
57. Oliveira G, Stromhaug K, Klaeger S, Kula T, Frederick DT, Le PM, et al. Phenotype, specificity and avidity of antitumour CD8+ T cells in melanoma. Nature. Nature Research; 2021;596:119–25.
58. Caushi JX, Zhang J, Ji Z, Vaghasia A, Zhang B, Hsiue EHC, et al. Transcriptional programs of neoantigen-specific TIL in anti-PD-1-treated lung cancers. Nature. Nature Research; 2021;596:126–32.

59. Lowery FJ, Krishna S, Yossef R, Parikh NB, Chatani PD, Zacharakis N, et al. Molecular signatures of antitumor neoantigen-reactive T cells from metastatic human cancers. Science. American Association for the Advancement of Science; 2022;375:877–84.
60. van der Leun AM, Traets JJH, Vos JL, Elbers JBW, Patiwael S, Qiao X, et al. Dual Immune Checkpoint Blockade Induces Analogous Alterations in the Dysfunctional CD8+ T-cell and Activated Treg Compartment. Cancer Discov. 2023;13:2212–27.
61. Raeber ME, Rosalia RA, Schmid D, Karakus U, Boyman O. Interleukin-2 signals converge in a lymphoid-dendritic cell pathway that promotes anticancer immunity. Sci Transl Med. 2020;12:eaba5464.
62. Buchbinder EI, Dutcher JP, Daniels GA, Curti BD, Patel SP, Holtan SG, et al. Therapy with high-dose Interleukin-2 (HD IL-2) in metastatic melanoma and renal cell carcinoma following PD1 or PDL1 inhibition. J Immunother Cancer. 2019;7:49.
63. Buchbinder EI, Gunturi A, Perritt J, Dutcher J, Aung S, Kaufman HL, et al. A retrospective analysis of High-Dose Interleukin-2 (HD IL-2) following Ipilimumab in metastatic melanoma. J Immunother Cancer. 2016;4:52.
64. Malek TR, Yu A, Vincek V, Scibelli P, Kong L. CD4 regulatory T cells prevent lethal autoimmunity in IL-2Rbeta-deficient mice. Implications for the nonredundant function of IL-2. Immunity. 2002;17:167–78.
65. Davidson TS, DiPaolo RJ, Andersson J, Shevach EM. Cutting Edge: IL-2 is essential for TGF-beta-mediated induction of Foxp3+ T regulatory cells. J Immunol Baltim Md 1950. 2007;178:4022–6.
66. Camisaschi C, Casati C, Rini F, Perego M, De Filippo A, Triebel F, et al. LAG-3 expression defines a subset of CD4(+)CD25(high)Foxp3(+) regulatory T cells that are expanded at tumor sites. J Immunol Baltim Md 1950. 2010;184:6545–51.
67. Pauken KE, Sammons MA, Odorizzi PM, Manne S, Godec J, Khan O, et al. Epigenetic stability of exhausted T cells limits durability of reinvigoration by PD-1 blockade. Science. 2016;354:1160–5.
68. Sen DR, Kaminski J, Barnitz RA, Kurachi M, Gerdemann U, Yates KB, et al. The epigenetic landscape of T cell exhaustion. Science. 2016;354:1165–9.
69. Yao C, Sun H-W, Lacey NE, Ji Y, Moseman EA, Shih H-Y, et al. Single-cell RNA-seq reveals TOX as a key regulator of CD8+ T cell persistence in chronic infection. Nat Immunol. 2019;20:890–901.
70. Khan O, Giles JR, McDonald S, Manne S, Ngiow SF, Patel KP, et al. TOX transcriptionally and epigenetically programs CD8+ T cell exhaustion. Nature. 2019;571:211–8.
71. Alfei F, Kanev K, Hofmann M, Wu M, Ghoneim HE, Roelli P, et al. TOX reinforces the phenotype and longevity of exhausted T cells in chronic viral infection. Nature. 2019;571:265–9.
72. Scott AC, Dündar F, Zumbo P, Chandran SS, Klebanoff CA, Shakiba M, et al. TOX is a critical regulator of tumour-specific T cell differentiation. Nature. 2019;571:270–4.
73. Beltra J-C, Abdel-Hakeem MS, Manne S, Zhang Z, Huang H, Kurachi M, et al. Stat5 opposes the transcription factor Tox and rewires exhausted CD8+ T cells toward durable effector-like states during chronic antigen exposure. Immunity. 2023;56:2699-2718.e11.
74. van den Brink SC, Sage F, Vértesy Á, Spanjaard B, Peterson-Maduro J, Baron CS, et al. Single-cell sequencing reveals dissociation-induced gene expression in tissue subpopulations. Nat Methods. 2017;14:935–6.

Supplementary figures

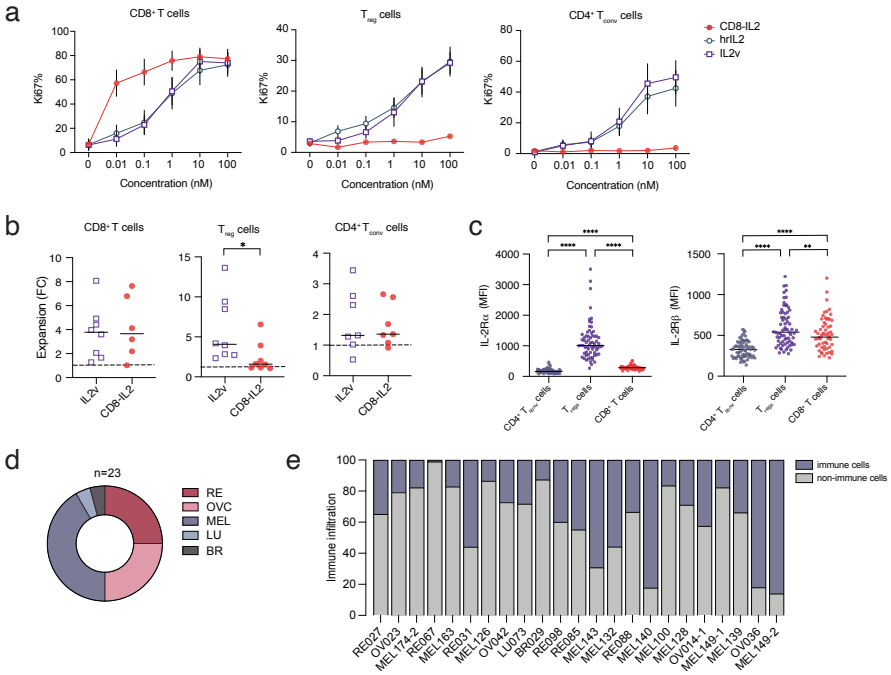

Figure S1. CD8-IL2 activates CD8⁺ T cells in human tumor samples with high specificity. (a) Ki67 staining of CD8⁺ T cells, CD4⁺ T cells and T_{regs} in human tumor digests (n=6) treated with human recombinant IL-2 (hrIL2), an untargeted IL-2 variant (IL2v) and CD8-IL2 at different concentrations. Data show mean +/- SEM. **(b)** T cell expansion of CD8⁺ T cells, CD4⁺ T cells and T_{regs} in human tumor digests upon five days of incubation with either IL2v and CD8-IL2 (at 10 nM concentration). **(c)** Expression levels (mean fluorescence intensities, MFIs) of IL-2 receptor subunits a (left) and b (right) by CD8⁺, CD4⁺ T cells and T_{regs} from multiple tumor types. **(d)** Cancer types included in the PDTF cohort (RE = renal cell carcinoma, OV = ovarian cancer, MEL = melanoma, LU = non-small cell lung cancer, and BR = breast cancer) **(e)** Quantification of immune infiltrates present at baseline assessed by flow cytometry within total live cells. *$P < 0.05$ by Mann-Whitney U test (b). ****$P < 0.0001$, ***$P < 0.001$ by Friedman test corrected for multiple comparisons (c). Only significant comparisons are shown (f).

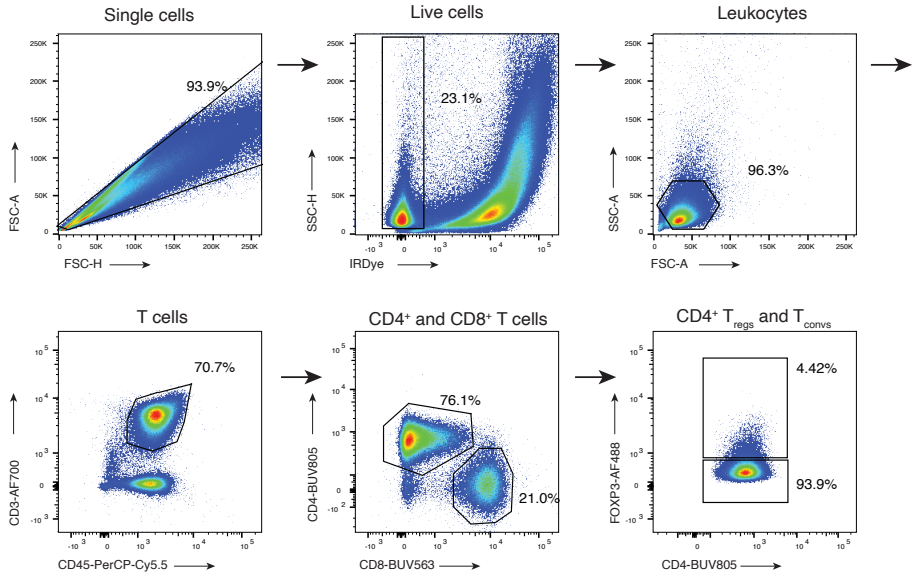

Figure S2. Gating strategy of PDTFs. Representative gating strategy of different T cell subsets in ex vivo cultured patient-derived tumor fragments used for flow cytometry analyses and cell sorting for single-cell RNA-sequencing analysis.

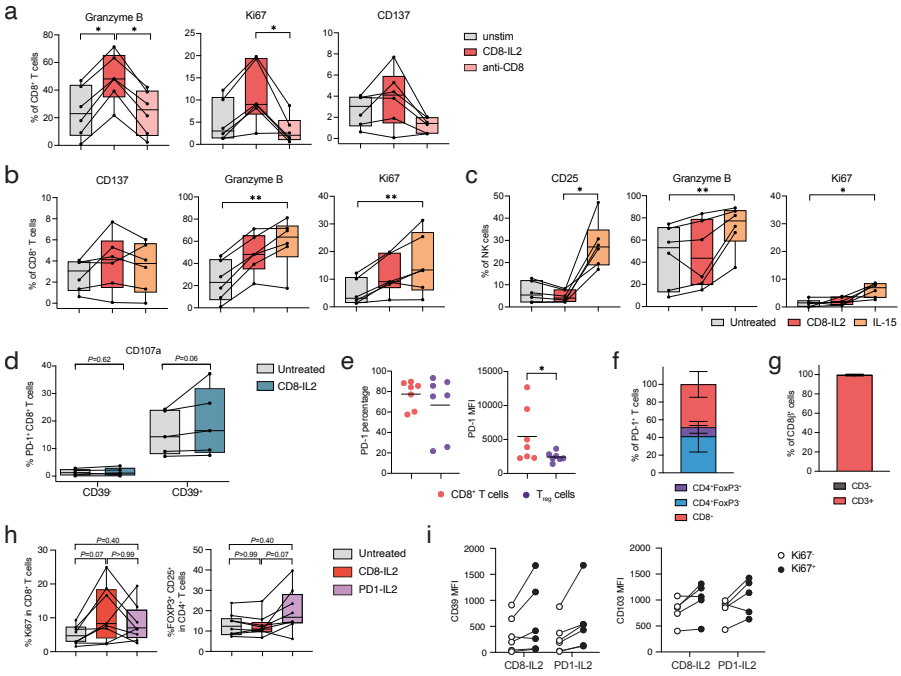

Figure S3. Comparison of CD8-IL2 induced T cell activation to anti-CD8, IL-15 and PD1-IL2 treatment. (a) Quantification of activation markers on total intratumoral CD8$^+$ T cells in untreated, CD8-IL2- or anti-CD8-treated PDTFs measured by flow cytometry (n=6). **(b+c)** Quantification of activation markers on total intratumoral CD8$^+$ T cells **(b)** and NK cells **(c)** in untreated, CD8-IL2- or IL15-treated PDTFs measured by flow cytometry (n=6). **(d)** Quantification of CD107a staining in human tumor digests left untreated or treated with CD8-IL2 for 6 hrs. separated for PD-1$^+$CD39$^+$ (late dysfunctional) and PD-1$^+$CD39$^-$ (early dysfunctional T cells). **(e)** Percentage and expression level of PD-1 on intratumoral CD8$^+$ T cells and T_{reg} cells. **(f)** Distribution of CD8$^+$, CD4$^+$ T_{conv} and CD4$^+$ T_{regs} within PD-1 expressing cells. **(g)** Distribution of CD3$^+$ and CD3$^-$ T cells within CD8b$^+$ T cells. **(h)** Ki67 staining in CD8$^+$ T cells and FOXP3$^+$CD25$^+$ staining in total CD3$^+$ T cells upon CD8-IL2 and PD1-IL2 in human PDTFs. **(i)** MFI of CD39 and CD103 in proliferating (Ki67$^+$) and non-proliferating (Ki67$^-$) intratumoral CD8$^+$ T cells upon CD8-IL2 and PD1-IL2. $^{**}P < 0.01$, $^{*}P < 0.05$ by Friedman test corrected for multiple comparisons. Only significant comparisons are shown (a-c, e, h). Only significant comparisons are shown (a-c).

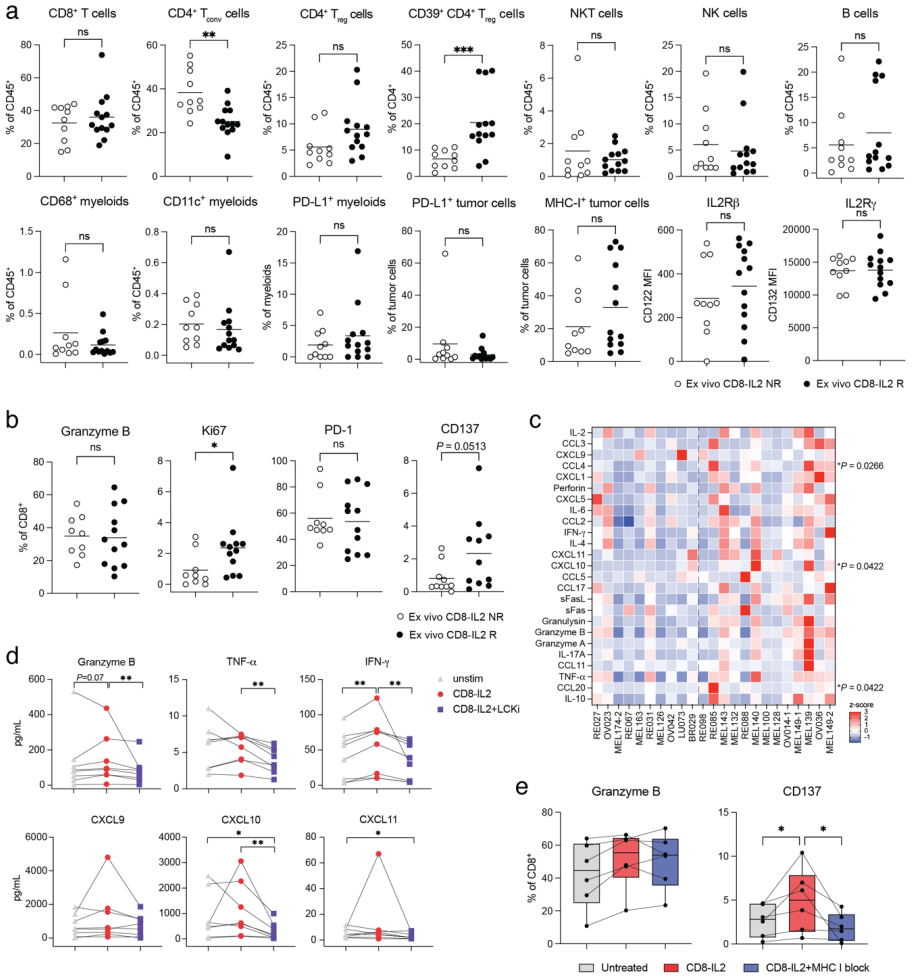

Figure S4. Baseline characteristics of CD8-IL2-R and -NR tumors. (a) Immune cell subsets present at baseline in ex vivo CD8-IL2 responding (n=13) and non-responding tumors (n=10). **(b)** Expression of activation markers in untreated PDTFs shown separately for CD8-IL2-R (n=12) and -NR (n=9) tumors. **(c)** Heatmap displaying normalized values of 25 soluble mediators secreted during steady-state culture in CD8-IL2-R (n=13) and -NR (n=10) tumors. **(d)** Examples of T cell effector cytokines (IFN-g, TNF-a), cytotoxic mediators (Granzyme B), and chemokines (CXCL9, CXCL10, CXCL11) in unstimulated, CD8-IL2, and CD8-IL2+LCKi stimulated PDTFs in ex vivo responding tumors. **(e)** Intratumoral $CD8^+$ T cell activation of CD8-IL2-R tumors upon CD8-IL2 and CD8-IL2+MHC class I blockade measured by flow cytometry (n=6). $^{***}P < 0.001$, $^{**}P < 0.01$ by Mann-Whitney *U* test (a-c). $^{**}P < 0.01$, $^{*}P < 0.05$ by Friedman test (d, e). Only significant comparisons are shown (d, e).

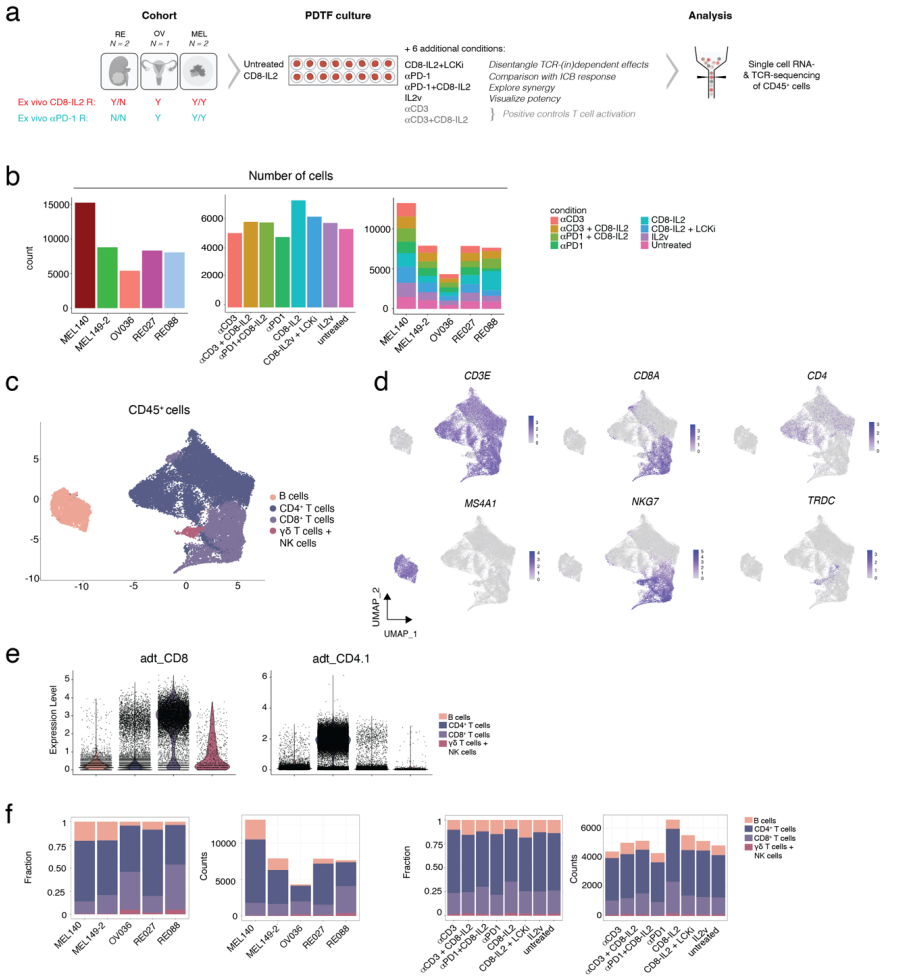

Figure S5. Single-cell RNA-sequencing (scRNAseq) design and analysis. (a) Overview of the cohort and experimental design of PDTF cultures used for scRNAseq. Positive control conditions (anti-CD3 and anti-CD3+CD8-IL2) were not included for downstream analysis of CD8⁺ T cells. **(b)** Number of cells recovered per tumor, per condition and per sequencing lane (one per tumor) showing the distribution of cells per condition. **(c)** UMAP of all immune cells sequenced. **(d)** Expression of key immune lineage genes overlayed on the UMAP. **(e)** CD8 and CD4 protein expression measured by CITE-seq antibodies in the different immune cell clusters from (c). **(f)** Fraction and counts of immune cell subsets in the different tumors and conditions.

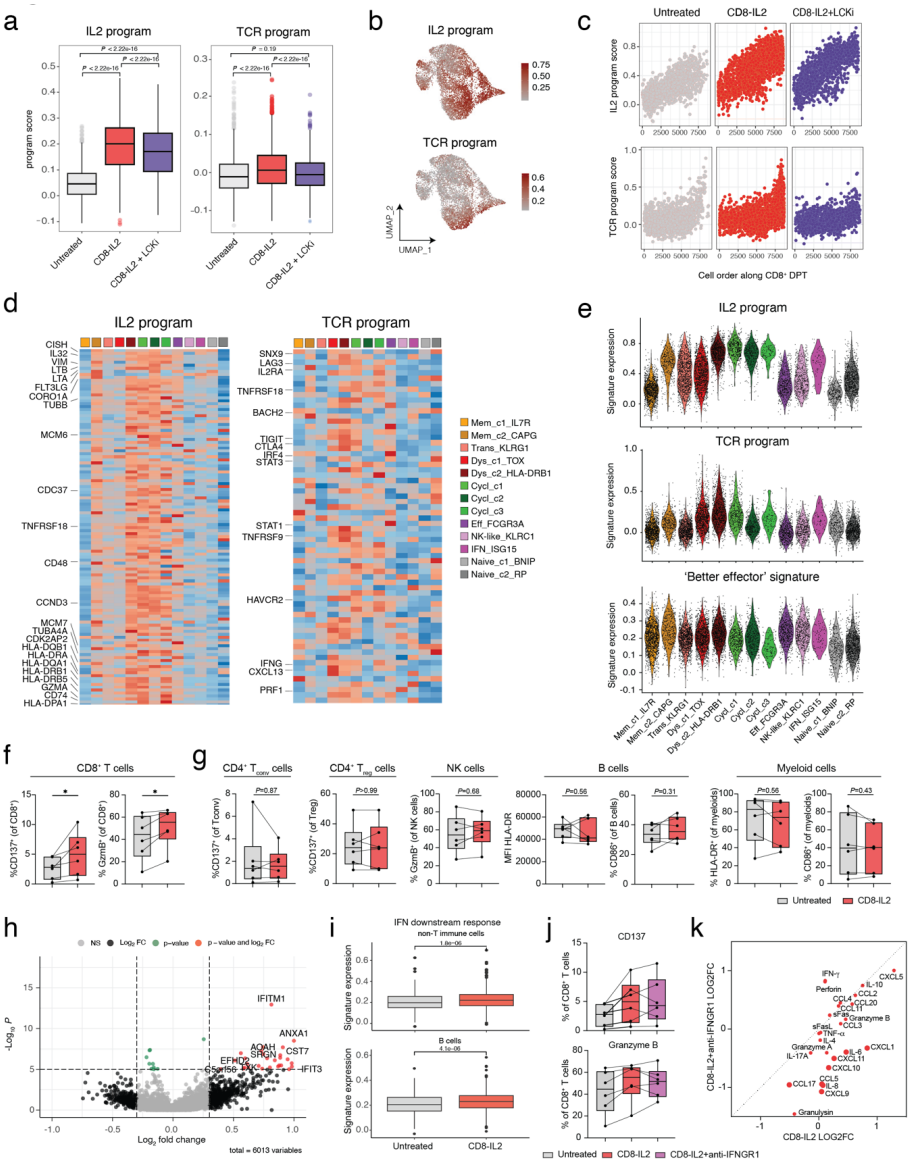

Figure S6. Annotation of transcriptomic states of intratumoral CD8⁺ T cells. (a) Cluster distribution of intratumoral CD8⁺ T cells from PDTFs before data integration. **(b)** Cluster distribution of intratumoral CD8⁺ T cells from PDTFs after data integration. **(c)** Heatmap of normalized expression of top10 differential expressed genes (DEGs) per CD8⁺ T cell cluster (Wilcoxon rank sum test). **(d)** Cell cycling scores for the S-phase (S.Score) and the G2M-phase (G2M.Score) for the cells in each cluster.

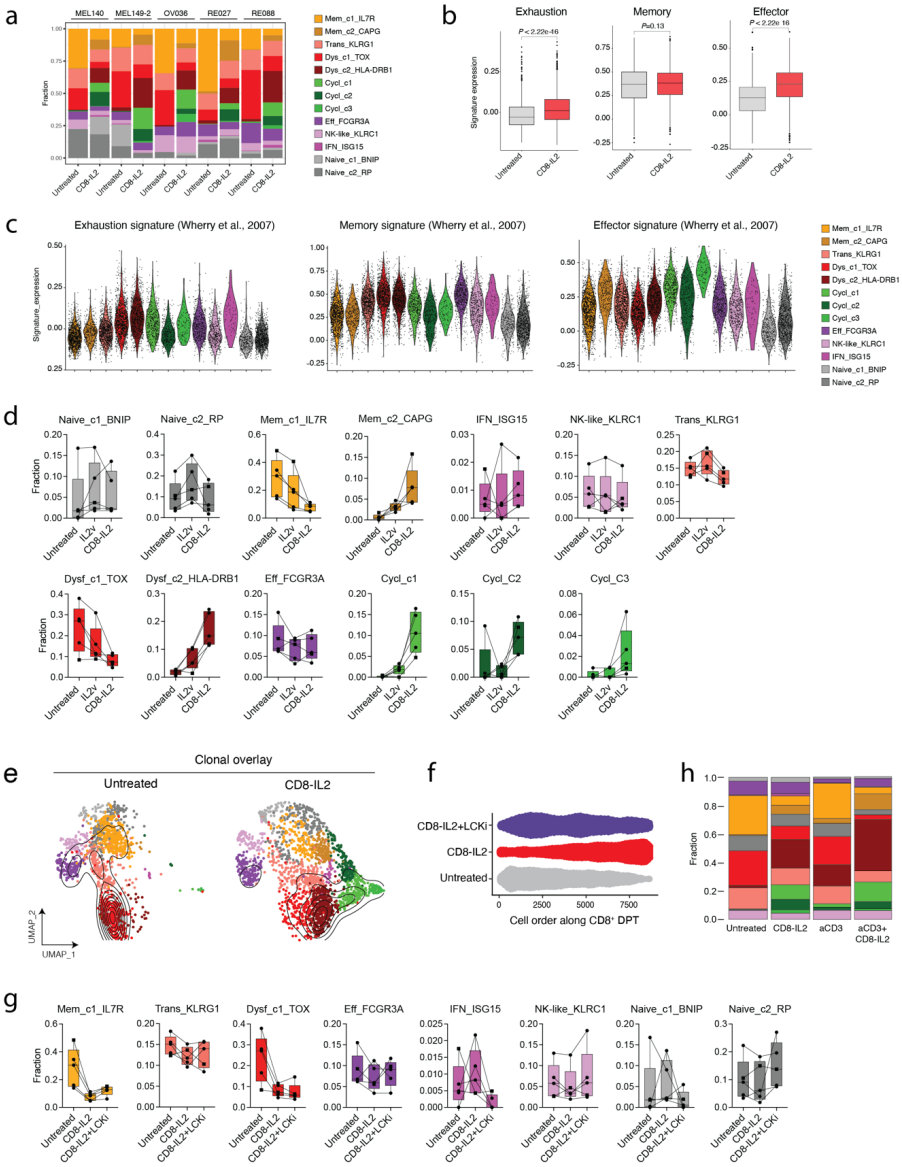

Figure S7. Response dynamics of intratumoral CD8⁺ T cell states to CD8-IL2 and other IL-2 conditions. (a) Cluster distribution of intratumoral CD8+ T cells from untreated and CD8-IL2-treated PDTFs shown for each tumor separately. **(b)** Expression of exhaustion, memory and effector signatures derived from Wherry *et al.*[55] in CD8⁺ T cells from untreated and CD8-IL2-treated PDTFs, and **(c)** in the different CD8⁺ T cell clusters. **(d)** Paired fractions of CD8⁺ T cell clusters in untreated, CD8-IL2-treated, and IL2v-treated conditions. The CD8-IL2 non-responding tumor (RE027) is marked by a square, the four responding tumors by circles. **(e)** Clonal overlay analysis displaying clonal expansion patterns for the untreated and CD8-IL2-treated conditions. **(f)** Diffusion pseudotime (DPT) for CD8⁺ T cells in the untreated, CD8-IL2, and CD8-IL2+LCKi conditions. **(g)** Paired fractions of CD8⁺

T cell clusters in untreated, CD8-IL2-treated and CD8-IL2+LCKi-treated conditions for the clusters not displayed in Fig. 5c. **(h)** Label transfer of clusters from the CD8-IL2 condition on intratumoral CD8⁺ T cells from anti-CD3 and anti-CD3+CD8-IL2-treated PDTFs. *P* values were calculated by two-tailed Wilcoxon test (b).

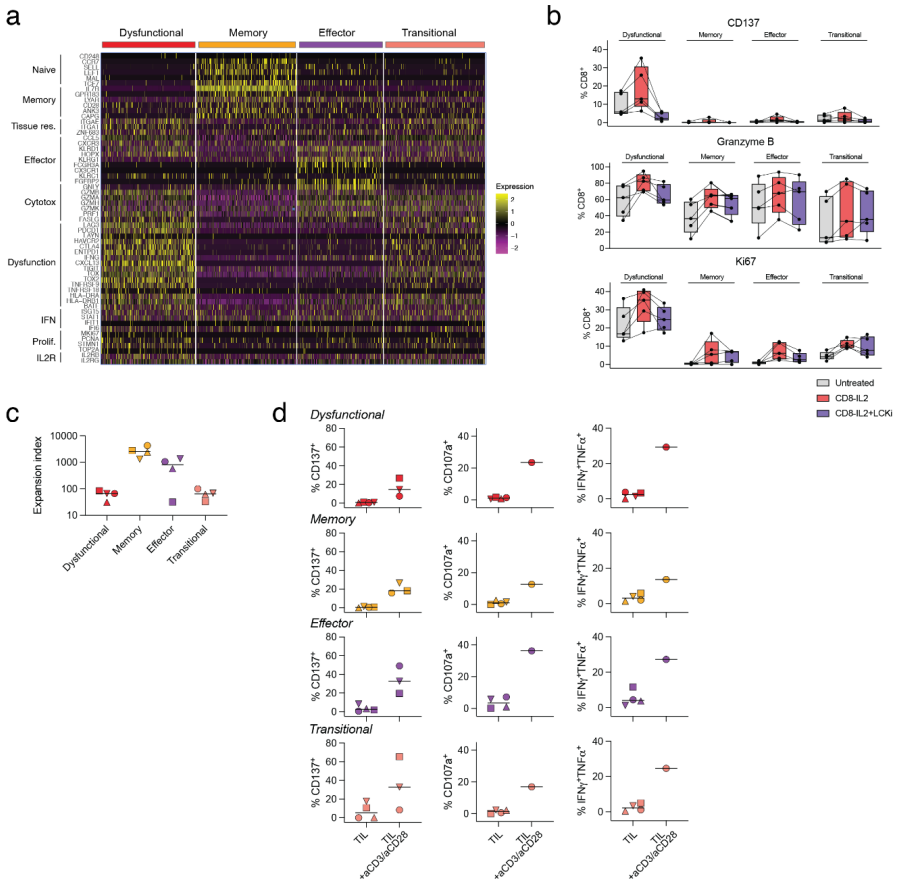

Figure S8. Characterization and tumor reactivity of sorted intratumoral CD8⁺ T cell populations. **(a)** Heatmap displaying canonical marker genes in sorted dysfunctional, memory, effector, and transitional CD8⁺ T cells. **(b)** Expression of activation markers on the four CD8⁺ T cell subsets in untreated and CD8-IL2-treated PDTFs measured by flow cytometry (n=5). **(c)** Expansion index after rapid expansion of the four different T cell subsets. **(d)** Expanded dysfunctional, memory, effector, and transitional CD8⁺ T cells cultured without or with anti-CD3+anti-CD28 stimulation. Activation was measured as CD137, CD107a, and IFNγ/TNF-α expression by flow cytometry. Note that due to differences in expansion, not all populations reached sufficient cell numbers for all experiments.

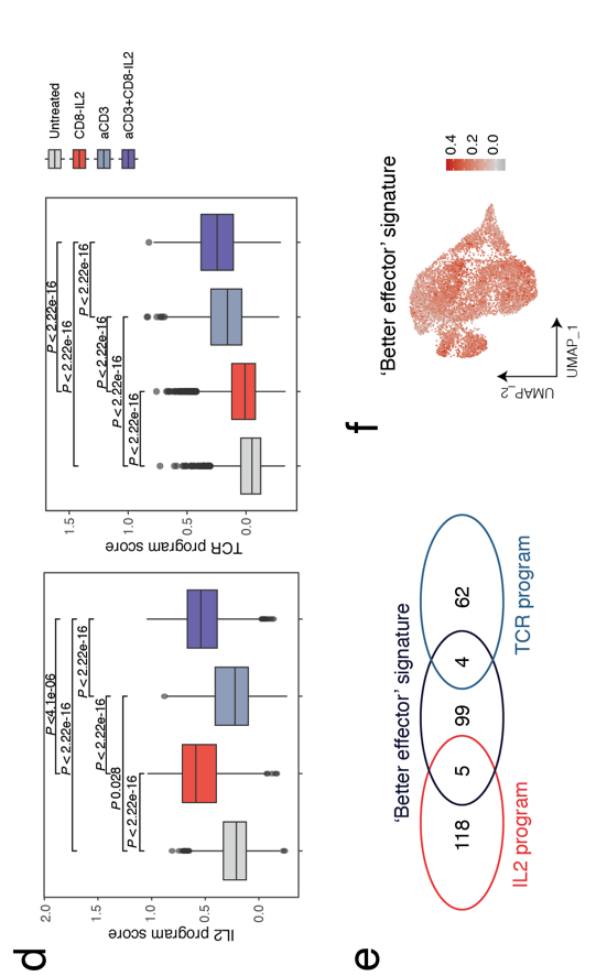

Figure S9. Development and expression of different gene programs capturing the CD8-IL2 induced effects. (a) Number of individual and overlapping genes between the IL2 and TCR gene programs. **(b)** Differential gene expression analysis between the untreated and the CD8-IL2+LCKi condition used for establishing the IL2 program. **(c)** Differential gene expression analysis between the untreated and the anti-CD3 condition used for establishing the TCR program. **(d)** IL2 program and TCR program scores in CD8$^+$ T cells from untreated, CD8-IL2-, anti-CD3-, and anti-CD3+CD8-IL2-treated PDTFs. **(e)** Number of individual and overlapping genes between the 'better effector' signature with the IL2 and TCR gene programs. **(f)** UMAP displaying the expression of the 'better effector' signature. *P* values were calculated by Wilcoxon test with Bonferroni correction for adjusted *P* values (b, c) and by two Wilcoxon test (d).

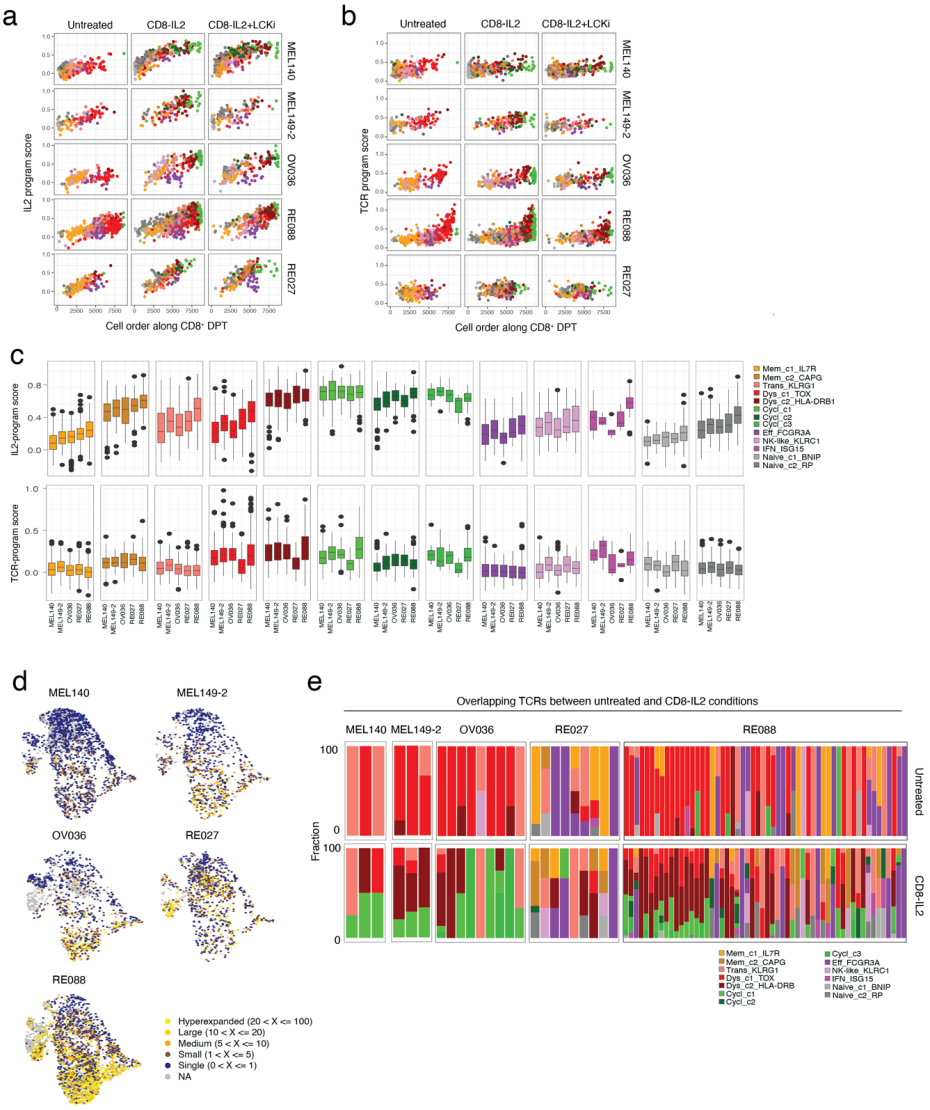

Figure S10. CD8-IL2-induced reinvigoration of intratumoral CD8⁺ T cells in individual tumor samples. (a+b) Expression of the IL2 program **(a)** and TCR program **(b)** in CD8⁺ T cells ordered along diffusion pseudotime (DPT) for the untreated, CD8-IL2, and CD8-IL2+LCKi conditions for each tumor individually. **(c)** IL2 program and TCR program scores for each cluster in each individual tumor. **(d)** UMAP of intratumoral CD8⁺ T cells displaying clonal expansion patterns for each individual tumor. **(e)** Cluster identity of overlapping TCRs that were present ≥1 times in the untreated and the CD8-IL2-treated condition.

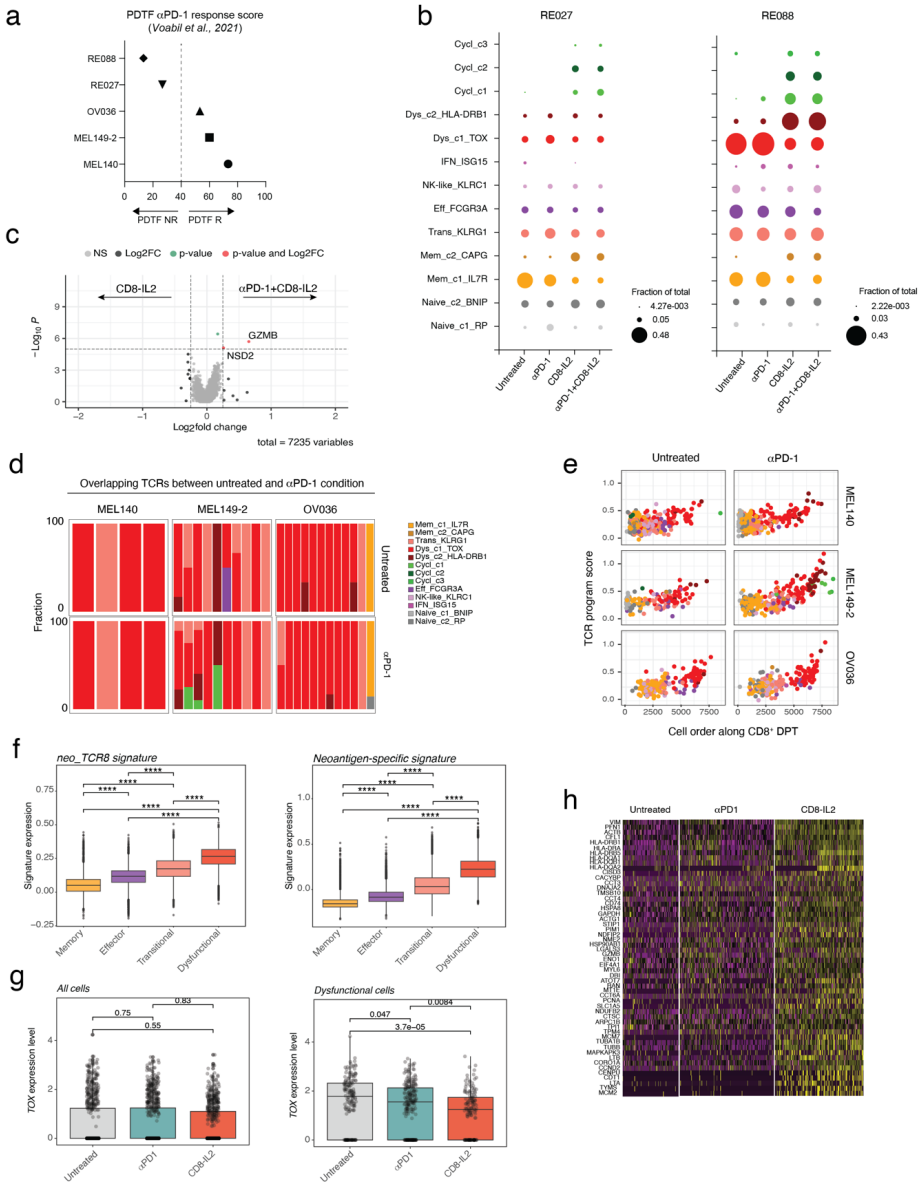

Figure S11. Comparison of intratumoral T cells responding to CD8-IL2 and to anti-PD-1. (a) PDTF score for ex vivo anti-PD-1 response (determined as described by Voabil *et al.*[10]) for the five tumors included in the scRNAseq analysis. **(b)** CD8⁺ T cell cluster distribution in PDTFs from the two anti-PD-1 non-responsive tumors that were untreated or treated with either CD8-IL2, anti-PD-1 or anti-PD-1+CD8-IL2. **(c)** Differential gene expression analysis of genes induced in the CD8-IL2 versus the anti-PD-1+CD8-IL2 condition for the three ex vivo anti-PD-1 responding tumors (OV036, MEL149-2 and MEL140). **(d)** Cluster identity of overlapping TCRs that were present ≥1 times in the untreated and the anti-PD-1-treated condition. **(e)** Expression of the TCR program in cells order along diffusion pseudotime from the untreated and anti-PD-1-treated conditions for each tumor individually. **(f)**

Neoantigen-specific gene signature score[51] and neo_TCR8 score[53] for the different sorted CD8⁺ T cell populations. **(g)** *TOX* gene expression levels in all CD8⁺ T cells and in the dysfunctional T cell pool in untreated, anti-PD-1-, and CD8-IL2-treated PDTFs. **(h)** Heatmap displaying most differentially expressed genes in tumor-reactive T cells from the untreated, anti-PD-1 and CD8-IL2 condition. *P* values were calculated by Wilcoxon test with Bonferroni correction for adjusted *P* values (c) and by two-tailed Wilcoxon test (f, g).

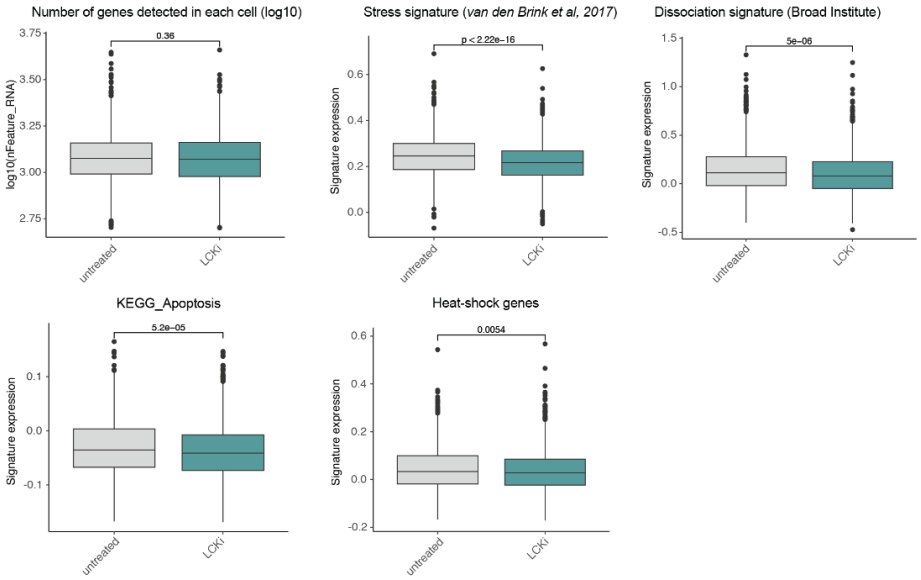

Figure S12. Characterization of LCKi-induced effects. Different gene expression signatures indicative of cellular stress, apoptosis and quality of the cells between cells from untreated and LCKi-treated fragments (n=2 tumors). *P* values were calculated by Wilcoxon test.